Reguzzi Simone (Orcid ID: 0000-0002-9461-7698)
Marini Mattia (Orcid ID: 0000-0002-4984-4074)
Zuffetti Chiara (Orcid ID: 0000-0002-7391-4829)

Stratigraphic evolution of a spectacularly exposed turbidite channel belt from the Tachrift System (late Tortonian, north-east Morocco)

Reguzzi, S. [1], Marini, M.[1*], Felletti, F.[1], Elkati I.[2], Zuffetti C.[1], Tabyaoui H.[2]

[1] Dipartimento di Scienze della Terra 'A. Desio', Università degli Studi di Milano, Milan, Italy.

[2] Natural Resources and Environment laboratory, Polydisciplinary Faculty of Taza, Sidi Mohamed Ben Abdellah University, Taza, Morocco

Corresponding author: mattia.marini@unimi.it

Keywords: *Channel bend expansion, channel morphodynamics, equilibrium profile, lateral accretion packages, turbidite channel, turbidite channel architecture*

Associate Editor – Victoria Valdez

Short Title – Controls on evolution of a turbidite channel belt

A ABSTRACT

The sedimentary architecture of channelized turbidites can be highly complex as it reflects the response of submarine channels to several interplaying factors. Although intensively investigated through seismic imaging, turbidite channel fills are not convincingly calibrated for sedimentary facies at a sub-seismic scale. This contribution addresses the sedimentary architecture and the controls on the evolution of a *ca* 20 m thick channel-levee complex of the Tachrift turbidite subunit (Upper Miocene, the Melloulou Formation), which accumulated along the southern slope of the Neogene Taza-Guercif Basin (Rifian Corridor of north-east Morocco). Facies and architectural analyses indicate that the studied channel-levee complex is the result of three-fold evolution. From base to top, it is comprised of: (i) a *ca* 7 m thick lower mud-prone interval containing relatively small and vertically stacked channel fills with poorly developed muddy levees, (ii) a *ca* 4 m thick and >1 km wide sandstone-rich middle interval made of lateral accretion packages that become progressively less amalgamated and fine-grained and is

This article has been accepted for publication and undergone full peer review but has not been through the copyediting, typesetting, pagination and proofreading process which may lead to differences between this version and the Version of Record. Please cite this article as doi: 10.1111/sed.13070

overlain by *ca* 5 m of thin-bedded mud-rich turbidites intercalated with hemiplegic marlstones, and (iii) an up to *ca* 9 m thick upper interval constituted by aggradational channel fills with well-developed levees and variously directed lateral accretion packages. This organization suggests that, following a phase of inception (lower interval), the channel underwent extensive meandering with very minor vertical aggradation, prior to being blanketed by 'retrogressive' muddy lobes (middle interval) during a phase of reduced sediment input. In turn, the uppermost interval records a late phase of channel re-establishment and aggradation that likely terminated as a result of up dip avulsion. It is suggested that the observed change of architectural style reflected the feedback of changing sediment input, slope equilibrium profile and channel morphodynamics.

A INTRODUCTION

Submarine channels are important geomorphological seafloor elements that traverse slopes and basin floors conveying sediments, organic matter, and pollutants transported by gravity flows into deep water (Peakall & Sumner, 2015; Kane & Clare, 2019). Up-dip, they can pass into a canyon that can incise deeply into the shelf edge and links to adjacent coastal and deltaic systems (e.g. Plink-Björlrklund & Steel, 2004). Although submarine channels are flushed from a range of flow types (from mass flows to highly dilute turbidity currents, locally modified by the action of contour currents; Peakall & Sumner, 2015; Fonnesu *et al.*, 2020), they are commonly referred to as turbidite channels. As a result of overbanking of the most dilute part of flows, turbidite channels are often laterally associated with levees, locally intercalated with crevasse deposits (Mutti, 1992; Peakall *et al.*, 2000; Posamentier & Kolla, 2003; Wynn *et al.*, 2007; Kane & Hodgson, 2011; Janocko *et al.*, 2013).

Although turbidite and fluvial channels show some morphological commonalities, their sedimentary processes are fundamentally different due to flow dynamics and a range of interplaying external controls, such as tectonics and sea level and sediment input changes (Peakall *et al.*, 2000; Kolla *et al.*, 2007; Sylvester *et al.*, 2011; Jobe *et al.*, 2016, 2020).

The planform of turbidite channels is commonly described in terms of sinuosity (i.e. ratio of the centre line length to the corresponding straight-line distance; Bridge, 2003). Sinuosity generally shows the tendency to vary down dip from relatively straight to sinuous (i.e. sinuosity greater than 1.05; Reimchen *et al.*, 2016) as the slope gradient reduces (Pirmez *et al.*, 2000; Kneller, 2003; Hodgson *et al.*, 2011), whereas tectonics and halokinesis can locally modify the slope resulting in more complex patterns (Pirmez *et al.*, 2000; Kane *et al.*, 2010, 2012; Covault *et al.*, 2020; Tek *et al.*, 2021). In meandering turbidite channels (*cf* with laterally accreting sinuous channels of Arnott *et al.*, 2021), sinuosity increases as a result of channel bend (or meander) expansion (i.e. swing; Peakall *et al.*, 2000). This results in accretion of inner bank apices with formation of point bar-like deposits is commonly referred to as lateral accretion packages (LAPs hereafter, Abreu *et al.*, 2003; Dykstra & Kneller, 2009; Pyles *et al.*, 2012), and contemporaneous erosion at the outer cut-bank (Babonneau *et al.*, 2010). Lateral accretion package deposition is promoted by a near-bed secondary flow (perpendicular to main flow direction) directed towards the inner bank cell circulation and apper to preferentially develop when turbidity currents are depleted in the intermediate grain size fraction (Arnott *et al.*, 2021).

The longitudinal depth profile and thus the planform of turbidite channels can also change over time because of the tendency of channels to attain a state of equilibrium at which their profile is characterized by a concave-up shape and the prevailing sediment discharge produces minimum aggradation or degradation (graded or equilibrium profile; Pirmez *et al.*, 2000). The tendency of channel to erode or aggrade at any point along its course, depends upon accommodation, which can be viewed as the space between the equilibrium profile (i.e. the slope profile of no net erosion or deposition) down the sediment transport pathway and the actual slope profile (Samuel *et al.*, 2003). The influence of flow parameters on submarine channel morphodynamics and sedimentation has been stressed by Kneller (2003) who proposed that, in a system at grade, changes in sediment input would induce adjustment of the along-dip channel profile to a new equilibrium. In this view, reduction in flow size, density

and efficiency should reflect in the tendency of a channel to aggrade. On the other hand, erosional channels would reflect a change towards higher efficiency, larger and denser flows.

Turbidite channels may initiate as relatively straight conduits dominated by erosion and bypass but rapidly undergo a phase of sinuosity increase in response to increasing sediment input (Elliott, 2000; Peakall *et al.*, 2000; Babonneau *et al.*, 2010; Hodgson *et al.*, 2011). Accompanied with LAPs development, this increse in sinuosity can be seen as an adjustment of the channel to changing flow condition, whereby meander growth will result in an increse of the channel legnht and a reduction of the local slope (Kneller, 2003). Upon reaching the equilibrium profile, channel sinuosity becomes relatively stable, even though its bends may be subject to downstream translation (sweep; Peakall *et al.*, 2000; Labourdette & Bez, 2010). At this stage, the channel tends to aggrade because it acts dominantly as a bypass zone (Peakall *et al.*, 2000), so that sweep result in superposition of LAPs with changing direction of accrection (e.g. Janbu *et al.*, 2007; Janocko *et al.*, 2013). Labourdette & Bez (2010) suggested that sweep may dominate over swing when channels are erosionally entrenched into older deposits or laterally confined by high-relief aggrading levees.

Based on numerous channel trajectory measurements from 21 turbidite channels, Jobe *et al.* (2016) have recently shown that adjustment of submarine channel systems to an equilibrium planform takes place in a two-phase evolution. The resulting depositional architecture commonly exhibits a 'hockey-stick' channel fill trajectory, whereby laterally stacked channel fills are gradually replaced upward by vertically staked channel fills.

Most of the understanding of how turbidite channels evolve has come from several decades of exploration of the seafloor and its subsurface, which has yielded incredibly detailed morphobathymetric and seismic imaging of present-day and hydrocarbon-bearing fossil examples (Weimer, 2000; Pettingill & Weimer, 2002; Weimer & Pettingill, 2007). Nonetheless, prediction of sub-seismic scale heterogeneity (below a few tens of metres) of channelized turbidites still relies on outcrop investigations (Sprague *et al.*, 2005; Wynn *et al.*, 2007; Janocko *et al.*, 2013; García *et al.*, 2015; Reimchen *et al.*, 2016; Gong *et al.*, 2020), which can

provide lithological and sedimentary facies calibration down to the scale of component event beds (Elliott, 2000; Navarro *et al.*, 2007; Kane & Hodgson, 2011; Pyles *et al.*, 2012; Arnott *et al.*, 2021).

Among the outcrop examples published to date, Elliott (2000) documented the stratigraphic variability of the Ross Sandstone Formation of western Ireland, recognizing an early incisional phase during which a low sinuosity channel with composite basal erosion (megaflute surface) was established, and a late depositional phase of channel-axis infill, lateral expansion, and development of higher sinuosity and laterally migrating channels with laterally accreted bedsets.

Navarro *et al.* (2007) detailed the architecture of an up to 90 m thick channel-levee complex from the Isaac Formation (Southern Canadian Cordillera). Correlations, detailing a bend of the channel belt, illustrate the stratigraphic transition from an inception phase dominated by axial bypass and development of low-relief asymmetrical levees to a mature stage of channel aggradation, during which continued levee growth is accompanied with an increased in-channel deposition. Navarro *et al.* (2007) also proposed that the observed architectural complexity may largely reflect sediment input variations at a range of scales.

In an investigation of channel-levee deposits from the Karoo Basin (South Africa), Hodgson *et al.* (2011) explained the stratigraphic transition from a basal master erosion to horizontally-stacked and then vertically aggraded channel fills as the response of an equilibrium profile shift from low to high accommodation conditions, through an intermediate phase of at grade profile.

The role of sediment input variations was emphasized by McHargue *et al.* (2011), who proposed that the stratigraphic heterogeneity of channelized turbidites is partly due to cyclic changes of gravity flow energy at multiple timescales (*cf.* with 'build-cut-fill-spill' sequences of Gardner & Borer, 2000). This results in alternation of phases of 'waxing', during which relatively large, highly concentrated and relatively coarse flows drive erosion of channel conduits bypassing most of their load, and 'waning' phases in which in-channel deposition

dominates as smaller volume, less concentrated and finer-grained flows are delivered to the system.

This paper investigates one of the several turbidite channel-levee complexes (Felletti *et al.*, 2020) belonging to the Tachrift System (*cf.* with Tachrift turbidite subunit of Gelati *et al.*, 2000) of north-east Morocco, which was deposited in the late Miocene as part of the sedimentary fill of the Taza-Guarcif Basin (Bernini *et al.*, 1999). The studied complex (Complex 4, hereafter) is *ca* 20 m thick and occurs halfway within the Tachrift System forming, together with the part of the complexes above and below and the intervening hemipelagic marlstones, a reverse polarity magnetozone (corresponding to the late Tortonian polarity Chron C3Br.2r; Krijgsman & Langereis, 2000) deposited in *ca* 151 kyr (Ogg, 2020). The aim of this paper is four-fold: (i) to document the stratigraphic variability of sedimentary architecture of a sinuous meandering slope channel at a sub-seismic scale; (ii) to highlight the possible role of sediment input variations on channel morphodynamics; (iii) to test current models explaining stratigraphic changes of channel trajectory and linked depositional patterns; and (iv) to constrain time duration of Complex 4 by providing lithological calibration of magnetobiochronology from literature.

To do this, Complex 4 was detailed through 84 closely spaced (*ca* 50 m) sedimentary logs which were correlated bed-by-bed to construct multiple architectural panels. Results reveal a vertical stratigraphic change in architectural and depositional style that, based on magnetobiochronology from literature (Krijgsman & Langereis, 2000), likely occurred over a time span of a few kyr. It is proposed that the observed sedimentary architecture, developed at a sub-seismic scale and thus potentially underappreciated in subsurface analogues, reflects the turbidite channel response to changes in sediment input occurring at a range of temporal scales. This study provides an unprecedentedly detailed record of the feedback of sediment input variation and turbidite channel morphodynamics, which may find application in forward modelling and prediction of sedimentary heterogeneity in analogue systems.

A GEOLOGICAL SETTING

The Taza-Guercif Basin of north-east Morocco (Fig. 1) is part of the Rifian Corridor (Flecker *et al.*, 2015; Capella *et al.*, 2018), a remnant of the Rif foreland basin system that acted as a seaway connecting the Atlantic Ocean to the Mediterranean sea during the late Miocene (Bernini *et al.*, 1999; Gelati *et al.*, 2000; Sani *et al.*, 2000; Capella *et al.*, 2017, 2019). Together with its westerly equivalents, i.e. the Gharb and Fes-Maknes basins (Fig. 1), the Taza-Guercif Basin was established since the early Tortonian as the result of a combination of flexural loading by the advancing thrust sheets of the Rifean system, and strike-slip tectonics in the Middle Atlas (Bernini *et al.*, 2000; Gelati *et al.*, 2000; Sani *et al.*, 2000; Capella *et al.*, 2017). These basins sit on top of a regional-scale unconformity which records the Cretaceous–early Miocene compressional reactivation of Jurassic rift faults of the Middle Atlas (Bernini *et al.*, 1999; de Lamotte *et al.*, 2009).

Marine transgression in the Taza-Guarcif Basin (Fig. 2A) started in the late Tortonian (Krijgsman *et al.*, 1999) with accumulation of the up to 500 m thick shallow marine Ras el Ksar Formation and it is locally preceded by deposition of the alluvial Draa Sidi Saada Formation (Benzaquen, 1965; Bernini *et al.*, 2000; Gelati *et al.*, 2000). The transgression culminates with the deposition of the Melloulou Formation (*The Tachrift turbidite subunit* section), a thick unit of interbedded hemipelagic marlstones and turbidites widespread in the Rifean Corridor (*cf.* with 'Marnes Bleues' of Benzaquen, 1965; 'Marnes Tortoniennes' of Colletta, 1977; 'Melloulou Unit' of Gelati *et al.*, 2000) and reflecting the maximum deepening of the Taza-Guercif Basin (Bernini *et al.*, 1999; Gelati *et al.*, 2000; Sani *et al.*, 2000; Krijgsman & Langereis, 2000). In the early Messinian, a tectonically controlled regression led to shallowing and then (from 6.7 Ma onward) emersion of the Taza-Guercif Basin (Krijgsman *et al.*, 1999; Krijgsman & Langereis, 2000; Capella *et al.*, 2017, 2018), with deposition of the gypsiferous Marls Subunit of the upper Melloulou Formation (Gelati *et al.*, 2000) and the shallow marine to continental Kef Ed Debe Formation (Sani *et al.*, 2000).

B The Tachrift turbidite subunit

In the southern Taza-Guercif Basin the Melloulou Formation includes the El Rhirane and the Tachrift turbidite subunits of Gelati *et al.* (2000) (Fig. 2B), which crop out to the west and to the east of the Zobzit river course, respectively, and were both fed from the south with sediments originating from the Middle Atlas (Pratt *et al.*, 2016). Although the relationship between these two turbidite subunits cannot be observed at outcrop due to faulting and extensive sediment cover by Plio-Quaternary deposits (Fig. 2A and B), geological mapping and structural reconstructions suggest that the Tachrift turbidite subunit is younger than the El Rhirane turbidite subunit (Gelati *et al.*, 2000).

The Tachrift turbidite subunit is a *ca* 600 m thick section (Zobzit Section, hereafter; Fig. 2C) of alternating channelized turbidites and hemipelagic marlstones (Bernini *et al.*, 1994; Gelati *et al.*, 2000). Magnetobiochronology investigations from the late 1990s (Krijgsman *et al.*, 1999; Krijgsman & Langereis, 2000) indicate that the Zobzit section was deposited between 7.7 Ma and 7.2 Ma with an accumulation rate that increased over time from 0.4 m/kyr (latest Tortonian) to 1.7 m/kyr (earliest Messinian). The 15 main turbidite layers reported by Krijgsman *et al.* (1999), have been recently mapped as nine channel-levee turbidite complexes (*sensu* Gardner *et al.*, 2003) by Felletti *et al.* (2020), who interpreted them as the product of a number of turbidite channel belts developed along the southern bounding slope of the Taza-Guercif Basin. Felletti *et al.* (2020) also distinguished four sedimentary facies associations, including sand-prone channel fills which can be further differentiated into amalgamated (channel axis association) versus non-amalgamated sandstones (channel-margin association), heterolithic levee deposits, mass transport deposits and hemipelagic marlstone, which locally contain methane-derived authigenic carbonates.

This work focuses on the *ca* 20 m thick Complex 4, which occurs half-way within the Tachrift turbidite subunit, sandwiched between hemipelagic marlstones. Together with Complex 3 and part of the Complex 2 below, the most of Complex 5 above and the intervening hemipelagic marlstones, Complex 4 forms a reverse polarity magnetozone (Fig. 2C), which was deposited during the polarity Chron C3Br.2r (between 7.305–7.456 Ma; late Tortonian) with an average

sedimentation rate of *ca* 1 m/kyr (Krijgsman & Langereis, 2000). Complex 4 is exposed along a *ca* 3.4 km long outcrop belt comprising three main outcrops, which in the following text will be referred to as southern, central and northern outcrops (Figs 3, 4 and 5).

A MATERIAL AND METHODS

Complex 4 was detailed acquiring and correlating 84 closely spaced (average spacing is *ca* 50m) sedimentary logs (Figs 3 and 6), which were measured making combined use of tape metre for individual beds thickness and a high-precision Jacob's staff with laser sighting capability (Patacci, 2016) for long-range measurements. Sedimentary log description was made with centimetre-scale resolution and included lithology, chart-aided estimations of grain size (i.e. using a grain-size comparator) and sorting, sedimentary structures, palaeoflow directions from sole and ripple marks, and bioturbation intensity. Correlation of adjacent logs was carried out tracking laterally continuous beds (Figs 4 and 5). On the other hand, sedimentary logs from different outcrops were correlated based on major sedimentary trends, after flattening them to a distinctive laterally continuous turbidite bedset (datum, hereafter) that occurs within the marlstones in between channel-levee complexes 4 and 5 (Figs 3 and 6).

Based on the Cullis *et al.* (2018) review of hierarchical classifications of deep-marine deposits, the following hierarchical ranks (Fig. 7A) will be used, which apply to both channel fill and correlative levee deposits. The term *single-storey* (‘*storey*’ *in brevis*; labelled with numbers in Fig. 6) is used to refer to a set of event beds deposited by a sequence of flows that progressively wax then wane in terms of their energy (McHargue *et al.*, 2011). A set of few to several storeys showing a common ‘migration’ pathway is here referred to as a *storey-set* (labelled with capital letters in Fig. 6; *cf.* with ‘composite channel’ of Gardner & Borer, 2000 and ‘channel fill’ of Sprague *et al.*, 2005). The term *complex* is used to refer to a higher-rank unit, bounded below and above by relatively thick packages of hemipelagic deposits, comprised of a stack of a few to several storey-sets. Finally, following Pickering & Cantalejo (2015), a stack of a few to several complexes separated by fine-grained marly deposits will be referred to as a *system* (for example, the Tachrift System).

Based on degree of bed amalgamation, bedding patterns and sedimentary facies, the sedimentary fill of relatively straight non-migrational 'cut-and-fill' channels are subdivided into axis, off-axis, and margin portions (Fig. 7B 'a). Conversely, channel fills made dominantly of laterally accreted sigmoidal bedsets, interpretable as lateral accretion packages formed at inner banks of sinuous meandering channels, are subdivided into toe-, middle- and top-sets (Fig. 7B 'b'). The toe-set constitutes the downlapping termination of the sigmoid, the middle-set encompasses the relatively thicker-bedded and inclined part of the sigmoid, whereas the top-set is the flat-lying upper portion of the sigmoid.

A RESULTS

B Sedimentary facies

On the basis of the dominant lithology, grain size, sedimentary structures and their vertical association, six sedimentary facies were identified (Table 1), including four sandstones facies (F1–F4) one mudstone facies (F5) and one chaotic, deformed facies (F6). Since bed and facies thicknesses are in most cases highly variable, in the following paragraphs thickness information will be provided in form of ranges, using the thickness classes of Campbell (1967) (Fig. 7A).

C Sandstones with a basal massive division (F1)

Facies F1 consists of medium to very thick beds of coarse to medium-grained sandstone, typically with scoured bases, which can include a basal mud-clast breccia (Fig. 8A and B). The basal division of F1 is represented by a massive interval, which may begin with traction carpets and normally grades upward into planar parallel (Fig. 8C) to ripple-laminated tops so as to form a T_{a-c} to T_{b-c} Bouma intervals. Less frequently, the basal massive division may be very thick and sharply overlain by a thin mudstone cap.

Facies F1 occurs almost exclusively as part of the sand-prone channelized units, although it may be sporadically found as single beds either in the marginal channel portions or in thin-bedded mud-prone units.

Interpretation: The basal division of F1 suggests that the rate of sediment fall-out from above was generally sufficiently high to suppress traction (Kneller & Branney, 1995; Kneller & McCaffrey, 1999). The upward transition to finer-grained laminated tops suggests deposition from a decelerating flow becoming less concentrated in time to result in establishment of traction plus fall-out conditions. Conversely, sharp capping of the very thick massive division (i.e. T_a) by a mudstone cap can be interpreted as evidence of bypass of the finer-grained sandy fraction carried by parent flows (Stevenson *et al.*, 2015).

C Cross-stratified sandstones (F2)

Facies F2 (Fig. 8D and E) consists of medium to thick, coarse to medium-grained, cross to trough-cross stratified sandstones (*cf.* with lower part of T division of Lowe, 1982). These sandstones pass upward, either sharply or more transitionally, to a mudstone cap, through a low angle to planar parallel-laminated division (*cf.* with Bouma T_b interval). F2 occurs mostly as part of the sand-prone channelized units and, more rarely, within the relatively muddier units separating subsequent single storey channel fills.

Interpretation: The cross-stratification suggests that F2 represents the product of two or three-dimensional small dunes forming underneath high-density flow conditions (Lowe, 1982, 1988; Arnott & Hand, 1989).

C Planar parallel-laminated sandstones (F3)

Facies F3 consists of medium to thick beds of normally graded medium to fine-grained sandstones characterized by a basal planar parallel-laminated division. The laminated basal division may either be sharply overlain by a co-genetic mudstone cap (facies F5) or, sometimes, grade upward into a rippled or convoluted top (Fig. 8F). More rarely, it passes upward to a structureless sandstone with abundant millimetre-sized mud-clasts.

This facies chiefly occurs as part of sand-prone channel fills, interbedded with facies F1 and F2, but can be also observed in heterolithic packages separating subsequent channel fills.

Interpretation: This facies shows similarities with T_{b-d} Bouma divisions with partly developed T_c-T_d intervals. It may be thus interpreted as the product of deposition from waning flows partly bypassing finer-grained sediments (Lowe, 1988; Mulder & Alexander, 2001).

C Thin-bedded bioturbated sandstones (F4)

Facies F4 consists of thin-bedded, fine- to very fine-grained sandstones which grade upward to their co-genetic mudstone cap. These beds generally show ripple to convolute lamination, although bioturbation and soft sediment deformation can commonly obliterate primary sedimentary structures (Fig. 9A and B).

Facies F4 is typically interbedded with mudstones (facies F5, see below) forming either parallel-stratified packages (Fig. 9A), correlative to sand-prone channel fills and interpretable as levees (Felletti *et al.*, 2020) or, less frequently, building cross-stratified bedsets in the uppermost channel fills (Fig. 7B).

Interpretation: This facies shows similarities with T_c and T_d–T_e Bouma divisions and can thus be interpreted to represent the product of deposition from low-density waning flows in relatively low-energy environments (for example, levees and channels at times of reduced sediment input), favourable to colonization by burrowing taxa (Bouma, 1962; Pickering *et al.*, 1986; Mulder & Alexander, 2001).

C Mudstone and marlstones (F5)

Facies F5 comprises turbidite mudstones and hemipelagic marlstones in variable proportions (Fig. 9C) and is interbedded to sandstone facies presented earlier in this section. Although weathering and soil formation makes unpractical to distinguish systematically turbidite mudstones from marlstones, it was possible to assess that the marlstone component is practically absent or only subordinate (less than 10%) in channel fills and associated with overbank deposits (see *Channel fills* and *Levee deposit* sections), while it is significant (*ca* 25%) in the relatively sandy thin-bedded interval that separates the middle from the upper part of Complex 4 (see *Muddy sheets* and *Central outcrop – lower and middle Complex 4* sections). Additionally, F5 can contain sparse concretions (Fig. 9D) and very thin beds of carbonate

micrite described earlier by Felletti *et al.* (2020), who interpreted them as authigenic carbonates deposited at biogenic methane seeps.

Interpretation: Facies F5 is interpreted as the result of fall-out deposition from the most dilute part of low-density turbidity currents (cf. Bouma T_e division and facies F9 of Mutti, 1992) and, secondarily, from suspended hemipelagic sediments.

C Chaotic, deformed deposits (F6)

Facies F6 occurs only in two instances, in the southern and the central outcrops (Fig. 6). In the southern outcrop, it overlays a relatively deep erosion (see *Southern outcrop* section) and is overlain by a few metres of thin beds of facies F4 and F5 (Figs 5D and 9E). It begins with an up to 1.5 m thick sandy conglomerate made of pebbles mostly of carbonate rocks (Fig. 9E and F), which is replaced upward by chaotic mudstones with scattered centimetre to decimetre-sized sandstone clasts and, higher on the erosion flanks, by chaotic marlstones.

Conversely, in the central outcrop, facies F6 is comprised of a slumped package of thin-bedded turbidites occurring atop the channelized deposits of storey-set D (Fig. 10), whose internal stratigraphy is in most part preserved and could be correlated to that of the nearby levee deposits.

Interpretation: The heterogeneity of facies F6 in the southern outcrop suggests deposition from a range of mass flows, including debris flows sourced axially (i.e. the conglomerate, Lowe, 1982) and mass wasting events shaping the erosion while this acted mostly as a bypass conduit (e.g. Qin, 2017; Counts *et al.*, 2021). On the other hand, the slump of the central outcrop is interpreted as the product of a mass wasting event involving the nearby levee (Fig. 11A, e.g. Picot *et al.*, 2016).

B Architectural elements and associated facies heterogeneity

C Channel fills

The sand-prone channel fills of Complex 4 shows a high variability of size (Table 2) and internal architecture. In the following sections, this variability will be addressed proceeding hierarchically, focusing first on single-storeys, and then on storey-sets.

D Single-storeys

Based on bed geometry, bedding patterns and facies distribution, two types of single-storey channels fills were recognized, namely '*cut-and-fill*' and '*laterally accreted*' single-storeys (see below in this section), representing the product of deposition in relatively straight channels versus sinuous meandering channels, respectively.

Common to both types of channel fills is the tendency of component event beds to become finer-grained, thinner, and less amalgamated proceeding from the older to the younger, which suggests single-storey formation may reflect sediment input waxing-waning cycles (McHargue *et al*., 2011; see *Introduction* section). As a result, the sandy and generally amalgamated part of single-storey channels fills is capped by thin-bedded muddy heterolithics (waning phase heterolithics; Fig. 7B), which include an increased proportion of marlstone and may be laterally contained by levees (Fig. 11A and B).

E 'Cut-and-fill' single-storeys. These channel fills were observed only in the lowermost part of Complex 4 (labelled as single-storeys 1–5), wherein they constitute relatively thin individual sand-prone bodies separated from one another by muddy heterolithics (Figs 6 and 10). They have lateral extents and maximum observed thickness in the ranges 200 to 450 m and 0.4 to 1.0 m, respectively, corresponding to aspect ratios varying from 185 to 1100 (Table 2). The base of these channel fills is erosional, cutting as deep as *ca* 1.5 m into the underlying mudstone and can show sole casts indicating northerly directed palaeoflow varying in the range 350 to 30°N. Channel fill tops are instead relatively flat, with a gentle dip towards the easterly quadrants (Fig. 10). Internally, the channel fill is made of few medium to thick sandstone beds with scoured bases, which stack vertically with no (for example, storeys 1, 4

and 5) or minor (for example, storey 2) lateral offset towards the east (for example, storey 2, Fig. 10). The sandstone beds making this type of channel fill are in most part amalgamated, but can also be heterolithic, thinner-bedded and finer-grained, as in the case of storey 5 (Fig. 10). The thickest axial parts of these channel fills are composed of amalgamated, massive and/or cross-stratified sandstone (facies F1 and F2, respectively). Away from the channel axes, less amalgamated and finer-grained beds are increasingly more common (for example, storeys 2–5, Fig. 10), comprising mostly cross-stratified, plane-parallel-laminated sandstone (facies F2 and F3, respectively), and rarely massive sandstone (facies F1), some of which were capped by very thin mudstones (facies F5).. Farther away from channel fill axes, off-axis deposits are replaced by very thin to thin-bedded channel margin heterolithics. These are alternations of planar parallel-laminated (facies F3), rippled (facies F4) and cross-stratified (facies F2) fine to very fine-grained sandstones with co-genetic mud caps (facies F5) (storey 4, Fig. 10). Centimetre-thick massive and cross-stratified sandstones (facies F1 and F2, respectively) may be present, suggesting occasional deposition by voluminous and relatively more concentrated flows (storeys 4 and 5, Fig. 10). Although basal grain size can vary from medium to very fine-grained sand from axial to marginal, there is generally little change in grain size across this type of channel fills.

Lastly, the waning-phase muddy heterolithics of 'cut-and-fill' storeys are represented by alternations of very fine-grained sandstone (dominantly facies F4), turbidite mudstones and marlstones (facies F5).

Interpretation: the lack of a distinct lateral accretion and inclined internal stratification/lamination such as those seen in laterally accreted storeys (see below) suggest that the formation of this type of channel fill progresses via subsequent slightly laterally off-set cut-and-fill events in relatively straight erosional channels (Fildani *et al.*, 2013). The less amalgamated parts of these channel fills reflect deposition in off-axis settings where sole erosion by subsequent flow was relatively minor. Although comparatively sandier and of larger-scale, analogue outcrop examples are those form the Tres Pasos Formation (Hubbard

et al., 2014), the Windemere Supergroup (Fraino *et al.*, 2022) and the Capistrano Formation (Camacho *et al.*, 2002).

E Laterally accreted single-storeys. These type of channel fills consist of sets of a few to several variably amalgamated sandstone beds that stack laterally with consistent inclined bedding. They have sigmoidal cross-sectional shape (Figs 11B, 11C and 12A) and can be interpreted as lateral accretion packages (LAPs hereafter; Abreu *et al.*, 2003).

Beautifully exposed examples of LAPs, cut at a range of angles with respect to the inferred direction of accretion, are those exposed in the central outcrop (for example, storeys 6–11; Figs 10 and 11), and in the northern outcrop (for example, storeys 13–17 and 22–23; Figs 12–14).

Although there is some variability in degree of sandstone amalgamation, mud-content and overall grain size, a typical facies association making LAPs can be summarized as follows.

The top-set facies association occupies the topographically higher part of the laterally accreted sigmoid, supposedly laying above the accreting inner channel bank (Fig. 7B 'b'). It is generally a few tens of centimetres thick and displays an along-dip continuity of up to a few tens of metres (Figs 11A and 12B). It comprises very thin to thick sandstone beds, either amalgamated (storey 8, Fig. 11A; storeys 13, 14 and 16 in Fig. 13) or partially preserving mudstone caps (storey 9, Fig. 11A and B; storey 14 in Fig. 14), which form fining-thinning upward sets. The most common sedimentary facies include, in varying proportions, massive (facies F1) and cross-stratified (facies F2) and, subordinately, horizontal plane-parallel-laminated (facies F3) and ripple-laminated (facies F4) sandstones.

The middle-set facies association constitutes the medial and thickest part of the sigmoid. It is composed of medium to very thick amalgamated sandstone beds (storeys 8–10, Fig. 11A and B; storeys 16 and 17, Figs 12 and 13), with thicknesses in the range 1.0 to 3.5 m and along-dip extents in the range 50 to 130 m. Because of the amalgamated nature of middle-sets, it appears that there is not a vertical pattern to grain size, facies and bed thickness. On the other hand, the most abundant sedimentary facies are in descending order, massive (facies F1),

cross-stratified (facies F2), planar parallel-laminated (facies F3) medium to coarse-grained sandstones (Fig. 13).

The toe-set facies association shows thicknesses in the range 0.1 to 0.5 m and along-dip lateral extents of few tens of metres (Fig. 11). It comprises very thin to thin beds of the full range of facies, generally organized into coarsening–thickening upward sets (storeys 8–10, Fig. 12; storey 23, Fig. 14).

Even though 3D stacking of component event beds result in very complicated pattern of basal and average grain-size variation, there is the tendency of middle-sets to represent the coarser part of LAPs. The base of middle-sets is also where most of the few observed sole casts were found and measured (for example, storeys 6–7 in Figs 10–11A and storeys 14 and 16 in Figs 13–14), returning a palaeoflow direction towards 345–35°N.

Waning-phase heterolithics of laterally accreted storeys are made of fine-grained planar parallel (facies F3) to ripple (facies F4) laminated sandstone with preserved mud caps, interbedded with minor proportions of hemipelagic marlstones (facies F5). These heterolithics tend to heal the pre-existing channel topography onlapping onto older deposits at both banks previously deposited LAPs and levees (storey 9, Fig. 11A and C).

Although subsequent erosion hampers establishment of the original lateral continuity and thickness of the majority of laterally accreted single-storeys, there is the tendency of these channel fill type to be comparatively larger than 'cut and fill' storeys, with widths and thickness in the range 300 to 554 and 0.74 to 2.54, respectively (Table 2).

Interpretation: Similarly to LAP examples from both the outcrop (Elliott, 2000; Navarro *et al.*, 2007; Wynn *et al.*, 2007; Li *et al.*, 2018; Arnott *et al.*, 2021) and the subsurface (Abreu *et al.*, 2003; Babonneau *et al.*, 2010; Labourdette & Bez, 2010; Janocko *et al.*, 2013; Reimchen *et al.*, 2016), laterally accreted storeys are interpreted to represent, together with the associated waning-phase heterolithics, the fill of sinuous meandering channels. The point-bar like geometry and internal organisation suggest accretion of the inner bank, promoted by inward

directed near-bed secondary flow circulation (Arnott *et al.*, 2021) chiefly during sediment input waxing phases.

D Storey-sets

Depositional shape (Table 2) and lithology of storey-sets can be highly variable, since they reflect the way a number of genetically related single-storey channel fills (locally with contrasting geometry, internal bedding pattern, and component lithofacies; see *Single-storeys* section) stacked spatially through channel belt evolution.

The coherent vertical stacking of storeys 2 to 5 suggests they represent part of a storey-set (storey-set θ, hereafter). Here, component storeys are separated each from another by waning-phase heterolithics (a few to several tens of centimetres-thick), are vertically stacked with minor lateral off-set, and are each associated to relatively muddy levees (see *Levee deposits* section). Together with the heterolithics laying immediately below and above, storey 1 may represent a storey-set on its own (storey-set Δ, hereafter), most likely developed at times of reduced sediment input.

Up-section, all other storey-sets (Figs 5 to 7 and 12), except for storey-set H, are similar for being made of variously amalgamated LAPs (see *Single-storeys* section) that, as detailed below, show a stratigraphic variability of accretion direction, spatial stacking and grain-size composition.

Storey-sets A and B are laterally stacked with minor aggradation and were most likely deposited in substantial continuity, as suggested by the lack of significant grain size and facies breaks in between. These are cut to the west by storey-set C (Figs 4C, 4D and 10), which represents the youngest of a few to several westerly storey-sets not detailed in this work because it is primarily exposed along an inaccessible cliff (Fig 4C). Erosionally based, storey-set C marks a westward relocation of the channel, which is accompanied with an up to 2 m deep erosion, suggesting a low sediment accommodation regime. Deposition continues with storey-set D, which is internally made of generally non-amalgamated and relatively finer-grained storeys (storeys 10–11; Figs 10 and 11). Although it could be argued that the less

sandy and amalgamated character of this storey-set is only apparent (the outcrop cut the channel fills in a marginal position and corresponds to toe or bottom-sets of a few to several storeys), its sandwiching between storey-sets A to C and the mud-prone thin-bedded succession above (see *Muddy sheets* section) rather suggests that it records a sediment input change towards less sandy and voluminous flows.

In storey-sets A to D, direction of accretion is mostly towards the east (storeys 8–9, Figs 10 and 11), although there are a few storeys (storeys 6 to 8, Fig. 10) in which bedding shows no apparent dip along the outcrop belt (i.e. these LAPs are cut along accretion strike), thus suggesting a more northerly or southerly directed accretion.

Differently from what observed in older storeys, the spatial stacking of storeys F, G and I record a mix of lateral stacking (or accretion) and aggradation, accompanied with coeval aggradation of correlative levees (see *Levee deposits* section) Conversely, the direction of lateral accretion seems to point towards the west in storey-sets F and G (for example, storeys 13 to 17 in Fig. 13), before changing again in storey-set I (for example, storeys 22–23 in Fig. 14), which displays a main component of accretion towards the east. However, it should be noted that, because of the aggradational nature of the upper Complex 4, early differential compaction can focus at certain locations so to make difficult to extrapolate direction of lateral accretion (Fig. 15).

As anticipated earlier, storey set H (Figs 13 and 14) is peculiar in that it shows no coherent lateral accretion, is heterolithic and relatively muddier and thinner compared to other storey-sets (Table 2). Sandwiched between storeys sets G and I, it can be widely correlated across the entire channel fill with little facies and thickness changes and is composed of small heterolithic storeys that tend to compensate the topography of the underlying deposit.

In terms of size, as a result of their laterally accreted motif, there is the tendency of laterally accreted storey-sets to be wider than the 'cut-and-fill' storey-set θ (Table 2).

C Levee deposits

The best exposed levee deposits of Complex 4 are associated with the storey-sets A to D (Figs 4B and 11A) and to the storey-sets F to I (Figs 5A, 13 and 14). The levee deposits of storey-sets A to D crop out to the south-east of these channel fills and are up to *ca* 3 m thick (Fig. 11A). These are made of muddy heterolithics with a sand-to-mud ratio of *ca* 0.25. They consist of very thin to thin beds alternations of fine-grained sandstone (facies F4) and, subordinately, plane-parallel-laminated fine to medium-grained sandstones (facies F3) and medium to thick beds of mudstone (facies F5). Based on the direction of lateral accretion of the channel fill sandstones (*Channel fills* section), these can be interpreted as outer bank levee deposits. These were locally prone to mass wasting, as suggested by the up to *ca* 1 m thick mildly deformed to chaotic heterolithic package (facies F6; see *Sedimentary facies* section) that occurs atop the channel fill of storey-set D (Fig. 11A), whose internal stratigraphy matches that of nearby levees.

The levee deposits of the storey-sets F to I are exposed on both sides of the correlative channel fills (Fig. 14), even though their best preservation is to the east (Figs 5A and 13), where they can be followed along-strike for *ca* 500 m. The westerly directed accretions of storey-set channel fills F and G (see *Channel fills* section) implies that the correlative heterolithics to the west and to the east might represent outer bank and inner bank levees, respectively (Figs 13 and 14). Component facies of the inner bank levees of these storey-sets are similar to those of storeys-sets A to D, although thicker and coarser sandstone beds are relatively more frequent, thickening towards the east. Consequently, the sand-to-mud ratio and cumulative levee thickness increase in the same direction from *ca* 0.25 to *ca* 1.1 and from 1.8 m to 2.8 m, respectively (Fig. 13). The thicker and coarser sandstone beds are up to 0.9 m thick and can be massive (facies F1), with horizontal plane-parallel-lamination (facies F3) and ripple cross-lamination (facies F4). Facies F1, F3 and F4 are separated by mudstone caps (facies F5) and stack vertically to form bedsets with a minimum lateral continuity of *ca* 600 m (Figs 13 and 14), locally characterized by coherent thickening-upward and coarsening-upward and then thinning-upward and fining-upward trends. Similarity with analogue deposits

interbedded with levee deposits (Beaubouef, 2004; Wynn *et al.*, 2007) suggests that these bedsets represent crevasse splays. If crevasse splay deposits are not taken into account, the sand-to-mud ratio is less than *ca* 0.45.

The outer bank levee of storey-sets F and G is only partly exposed, but its upper part appears devoid of sand intercalations interpretable as crevasse splay deposits and is characterized by a sand-to-mud ratio of *ca* 0.22.

The easterly-directed accretion of the storey-set channel fill I indicates that the correlative heterolithics to the west and to the east may represent inner and outer bank levees, respectively (Fig 14). The inner bank levee shows a sand-to-mud ratio of *ca* 0.4 and a thickening–coarsening to thinning–fining upward trend. Conversely, the outer bank levee is up to 2.8 m thick in the most proximal section and thins to 2.2 m over a distance of *ca* 70 m to the east, while the sand-to-mud ratio decreases from 0.18 and 0.07 (Fig. 14).

In the relatively less sandy storey sets Δ and θ, correlating bed-by-bed channel fill sandstones to coeval overbank deposits is impractical due to regolith cover (Fig. 4A). Nonetheless, observations made on the heterolithics cropping out sparely on both sides of 'cut-and-fill' storeys 2 to 5 (Fig. 10) suggest these channels fills have coeval poorly developed levees (elevation of the levee crest above the corresponding channel base was hardly greater than 1 m) with a sand-to-mud ratio less than 0.1.

In summary, correlations and lithological fraction estimation show that levees of Complex 4 become relatively sandier upward (i.e. storey sets A-I) and appear muddier on outer banks.

C Muddy sheets

These deposits occur sandwiched between storey-sets D and F and are exposed both in the upper part of the central and southern outcrop and in the lower part of the northern outcrop (Figs 4 and 6). They form a *ca* 5 m thick monotonous planar parallel stratified package that extends laterally for at least 2.5 km without significant change in sand-mud ratio and contains relatively small sandy channel fills (for example, storey-set E and storey 12; Figs 6, 10 and 13). They are mostly represented by non-amalgamated very thin beds of facies F4 and

subordinately by plane-parallel-laminated (facies F2), cross stratified (facies F3) and massive (facies F1) sandstones. Turbidite mud caps are generally thicker than the sandstone below and can pass upward to hemipelagic marlstones. The latter represent *ca* 25% of cumulative mudstone thickness of the entire section, suggesting a turbidite accumulation rate lower than elsewhere in Complex 4. Although the mudstone (i.e. turbidite and hemipelagic) fraction is significant, if the marly component is removed, these deposits turn out to be much sandier (sand-to-mud ratio is *ca* 55%) than levee deposits.

Interpretation: Occurring above the fining and less amalgamated up-ward channel fills of storey-sets A to D, this sedimentary unit is interpreted as deposition by dilute waning flows. Although some relatively thin bedsets are correlative to the channels fills of storey-set E and storey 12 (Fig. 6), and should thus be interpreted as levee deposits, the majority of beds are too sandy and volumetrically abundant to represent levee or crevasse splays deposits of channel fills occurring out of the studied section, suggesting they most likely represent muddy turbidite lobes (or the distal fringes of sandier lobes). These lobes blankets the preceding channel belt and might have formed during a relatively prolonged phase of reduced turbidite input, which resulted into backstepping of the turbidite system. In this view, the channelized storey-set E and storey 12 may be interpreted as the fills of short-lived channels that reached this far during shorter-term phases of waxing of prevailing sediment discharge.

B Large-scale architecture

Based on correlation of the southern, central and northern outcrops (Figs 3 and 6), this section provides a summary of large-scale architecture of Complex 4 (Fig. 16).

C Central outcrop - lower and middle *Complex 4*

The oldest deposits of Complex 4 are represented by the relatively small and muddy storey-sets Δ and θ (Fig. 16). These are made of single storey channel fills of the 'cut-and-fill' type (see *Single-storeys* section) that are stacked vertically with a slight westward off-set and are sided by poorly develop muddy levees (Figs 4A and 10).

Stratigraphically upward, laterally accreted channel fills (storey-sets A–D; Figs 6 and 10) stack spatially to form a *ca* 4 m thick and at least *ca* 1100 m wide sandstone-rich unit (its width exceeds that of the central outcrop; Figs 3 and 6), which to the east fringes into correlative levees (Fig 16; see *Levee deposits* section). Widely amalgamated in its lower part (storey-sets A–C), this channelized unit becomes less amalgamated and sandy upward (storey-set D), thus suggesting a sediment input change towards less sandy and voluminous flows prior to establishment of the 'retrogressive' muddy turbidite lobes above (see *Muddy sheets* section).

C Northern outcrop - upper Complex 4

The upper part of Complex 4 is superbly exposed in the close proximity of the western bank of the Zobzit river (Figs 3 and 5A to C). It is up of *ca* 9 m and comprises the laterally accreted storey sets I to F, which are vertically stacked (Figs 13–15) and make transition to levees both to the west and the to the east (Fig. 16). To the east, the levee deposits include several thicker sandstone beds that could be correlated with the upper section exposed in the central outcrop and are interpreted as crevasse deposits (see *Levee deposit* section).

Spatial stacking and cumulative thickness of channel fills, together with their relationship with time-equivalent levees, suggests the upper Complex 4 record deposition in an aggradational channel with well-developed levees.

C Southern outcrop

Here, Complex 4 begins with laterally migrating and accreted storeys that form several storey-sets (not detailed as part of this study, Fig. 16) with thicknesses, sedimentary facies and stratigraphic arrangement resembling that of storey-sets A to E from the central outcrop. Below these storey-sets, no channelized facies had been observed that could have been correlated to storey-set θ. The continuity of the laterally accreted bodies correlatable to storey-sets A to E is interrupted by a 5 m deep channelized erosion with a *ca* north–south oriented axis (Fig. 5C). This erosion is initially infilled with debris flow and *en masse* deposits (*Chaotic, deformed deposits* section) and subsequently with fine-grained thin-bedded turbidites. The relationship between this deep erosion and the northernmost outcrops is poorly constrained, but if the

datum plane used for flattening correlations is tilted to account for the slope dip (assumed to be in the order of 0.2°, Fig. 16), the position of the deepest point of the erosion is at a height similar to that of the aggradational upper part of Complex 4 (i.e. storey-sets F–I; see *Northern outcrop – upper Complex 4* section). This suggests that the erosion and its sedimentary fill may postdate deposition of the youngest stratigraphy of Complex 4 and thus relate to the latest phase of channel evolution (*Phase 3: channel re-establishment, aggradation and abandonment* section).

A DISCUSSION

B Stratigraphic evolution of Complex 4

The character and spatial arrangement of the architectural elements recognized in Complex 4 (Fig. 16) can be used to infer changes of channel morphodynamics and their likely controls. The stratigraphic evolution of the Complex 4 is three-fold and includes a phase of channel inception (Phase 1), a phase of extensive channel meandering and then blanketing by muddy lobes (Phase 2), and a late phase of channel re-establishment, aggradation and abandonment (Phase 3).

C Phase 1: channel inception

Complex 4 begins with the relatively small sandy fills of five erosional channels (storeys 1–5; corresponding to storey-sets Δ and θ; Figs16 and 17A) that, although not contained within a master erosion, are vertically stacked with minor lateral off-set. Separated from one another by metres-thick waning-phase heterolithics and are associated with poorly developed muddy levees, single-storeys 1 to 5 can be unequivocally recognized as the product of as many waxing–waning cycles of sediment input (McHargue *et al.*, 2011) through which a relatively stable, non-meandering channel was established. The vertical stacking of storeys 1 to 5 suggests that in subsequent waxing-phases the denser and erosive part of the flow was trapped within the under-filled (though veneered by waning-phase heterolithics) channel form of the preceding storey. These channel fills might thus represent the down-dip continuation of a relatively more erosional channel (e.g. Cronin *et al.*, 2000; Navarro *et al.*, 2007; Marini *et al.*,

2020; Fig. 17), which was established as sediment gravity flows were first delivered to the slope and remained active through multiple waxing-phases. It is reasonable to assume that the channel hosting deposition of storeys 1 to 5 progressively lost confinement down-stream, passing into a more distributive channel network associated to a dispersed and offset stratigraphic pattern of channel fills (Labourdette & Bez, 2010; *cf*. with 'disorganized pattern' in McHargue *et al.*, 2011; Funk *et al.*, 2012).

Similarly, although of larger scale, relatively straight erosional channels has been recognized to have initiated the modern Congo system (Babonneau *et al.*, 2010), the Pleistocene Mississippi system (Peakall *et al.*, 2000), the Lucia Chica Channel system off-shore central California and the fossil channelized Tres Pasos Formation of Chile (Fildani *et al.*, 2013), and the late Pleistocene Y channel of the western Niger Delta slope (Jobe *et al.*, 2015). Even though lacking discrete erosional channels such as those inferred to explain deposition of storey-sets Δ and θ, other outcrop examples featuring an inception phase dominated by erosion and bypass are reported by several authors (Elliott, 2000; Navarro *et al.*, 2007; Hodgson *et al.*, 2011).

C Phase 2: channel meandering and blanketing by muddy sheets

Up-section, Complex 4 continues with variously amalgamated laterally accreted channel fills (storey-sets A–D), in which widespread presence of LAPs indicate deposition in a sinuous meandering channel (Fig. 16).

Direction of LAP accretion indicates that storey-sets A and B were deposited in continuity on the inner bank of a bend that was expanding, contemporaneously with accumulation of relatively thin levee deposits on the outer bank (Figs 10 and 17B). Storey-set C marks a relocation of the channel to the west, most likely as a result of up-dip avulsion. This was followed by a further phase of east-directed bend expansion, with consequent accretion of the inner bank and erosion of storey-sets A and B at the outer bank (Fig. 17B). The direction of LAPs and the decrease in grain size and sandstone amalgamation from storey-set C through to storey-set D would suggest that, although continuing its westward expansion, the channel

started to slightly aggrade, as progressively finer sediments were delivered to the system. This reduction of sediment input would culminate in establishment of the 'retrogressive' muddy lobes (see *Muddy sheets* section) that blanketed the storey-sets A to D channel belt and were crossed by relatively small and short-lived channels developed during brief lapses of increased sediment input (Figs 16 and 17C).

The laterally extensive nature of the sand-prone package of storey-sets A to D suggests that it encompasses a relatively prolonged phase of channel meandering, accompanied with very little aggradation and arguably significant sediment bypass of at least the finer grained component carried by flows.

Laterally migrating channels producing laterally extensive LAPs similar to those of storey-sets A to D have been widely documented both in outcrop (Elliott, 2000; Abreu *et al.*, 2003; Navarro *et al.*, 2007; Wynn *et al.*, 2007; Li *et al.*, 2018; Arnott *et al.*, 2021) and in the subsurface (Babonneau *et al.*, 2010; Labourdette & Bez, 2010; Janocko *et al.*, 2013; Reimchen *et al.*, 2016), and generally are interpreted to reflect low sediment accommodation regimes or, alternatively, an early phase of channel gradient adjustment due to increasing sediment discharge (Kneller, 2003).

C Phase 3: channel re-establishment, aggradation and abandonment

The uppermost section of Complex 4 records a re-establishment of a sinuous meandering channel, which from now onward will aggrade contemporaneously with its levees (storey-sets F–I; Figs 16 and 17D). As result, LAPs show a significant aggradational trajectory and are subject to stratigraphic changes in direction of accretion (for example, see the contrasting direction of accretion of storey-sets F, G and I; Fig. 15). This indicates that while expanding within the confining levees, channel bends were subject to down-stream swing. Similar aggradational architecture, with vertically stacked LAPs with contrasting direction of accretion, has been documented at different scales, both in outcrop (for example, the Kusuri Formation from the Sinop Basin of Turkey; Janbu *et al.*, 2007) and in the subsurface (Babonneau *et al.*, 2010; Labourdette & Bez, 2010; Janocko *et al.*, 2013).

Aggradational channels forms in high accommodation regimes in the lower course of relatively steep out-of-grade systems (Pirmez *et al.*, 2000; Kneller, 2003; Samuel *et al.*, 2003; Hodgson *et al.*, 2011) and up-dip of topographic obstacles (growing tectonic or salt-related structures, mass transport deposits, and a combination thereof) due to flow blocking by (Kane *et al.*, 2012; Hansen *et al.*, 2015, 2017; Torres Carbonell & Olivero, 2019; Watson *et al.*, 2020; Park *et al.*, 2021; Tek *et al.*, 2021) or in systems at grade in which an equilibrium sinuosity has been reached and overspilling of finer-grained sediments promote levee aggradation (Peakall *et al.*, 2000). Alternatively, Kneller (2003) proposed that changes in flow parameters towards less dense, thick, and finer-grained flows might force a channel to aggrade, irrespective of the its along dip profile.

In the central and northern outcrops, Complex 4 ends with blanketing by hemipelagic marlstones (Figs 16 and 17D). Even though regolith cover hampers tracking to the north the channelized erosion characterizing the southern outcrop (Fig. 16; see *Southern outcrop* section), the stratigraphic position of this erosion (above storey-sets A–E and below the datum) suggests it might correlate to the abandonment (and subsequent blanketing by marlstones) of the aggradational channel of storey-sets F to I. Particularly, it can be speculated that this conduit first established following up-dip avulsion (Fig. 17D), deepened while transferring sediment gravity flows towards a lower-lying seafloor to the north/north-east, and was finally backfilled with dominantly fine grained turbidites during a subsequent sediment input waning-phase.

C Time-duration of Complex 4 and its building blocks

The time duration of Complex 4 can be loosely estimated based on the magnetochronology of Krijgsman & Langereis (2000), who correlated the *ca* 160 m thick reverse polarity package containing it to Chron C3Br.2r. This corresponds to an average depositional rate of *ca* 1 m/kyr that, however, encompasses both the hemipelagic and the turbidite components of the Tachrift System. Based on mapping by Felletti *et al.* (2020), field observations and measurements made as part of this work, it can be estimated that the marlstone component represents at

least half of the cumulative thickness of the Chron C3Br.2r magnetozone. Since rates of accumulation of channelized systems (Flood & Piper, 1997; Jobe *et al.*, 2015) are at least one order of magnitude greater than those of hemipelagic deposition on slopes (0.1–0.6 m/kyr; Hiscott, 1978), it can be concluded that Complex 4 might have accumulated at an average rate of a few metres per kyr during a time interval with a maximum duration of several kyr. Similar accumulation rates have been reported from modern (up to 25 m/kyr in levees of the Amazon fan and in the range of 1.6 to 20 m/kyr in channel Y of the Niger western slope; Flood & Piper, 1997; Jobe *et al.*, 2015) and outcrop examples (Daniels *et al.*, 2018; Englert *et al.*, 2020) of slope channels and a number of non-channelized turbidite systems (*cf*. Payros & Martínez-Braceras, 2014; Catuneanu, 2019, 2020; Marini *et al.*, 2020).

While in agreement with conclusions of Krijgsman *et al.* (1999), who suggested that alternation of turbidite and marlstone deposition in the Tachrift turbidite subunit might reflect precession cycles, the estimated time duration of Complex 4 highlights that, from inception to abanodnment, its parent channel belt developed over a relatively short span of a precession cycle. Whether this correlated to a period of increased run-off as suggested by Krijgsman *et al.* (1999) or a phase of sea-level lowering is unclear and needs further work. The estimated time duration of Complex 4 also has implications on the sedimentary meaning of the hierarchical orders documented in this work. If the majority of the storeys and storey-sets making up Complex 4 (at least 23 and 11, respectively, considering that some from the meandering phase are not preserved due to erosion) were actually the result of sediment input waxing–waning cycles, these might have formed at time scales of a few to several hundred years, respectively and therefore reflect shorter-terms changes in run-off and sediment export to the slope.

These results are novel in that they provides constraints on time-duration of a range of hierarchical ranks (i.e. from storey to complex and above) of turbidite channel architecture (Cullis *et al.*, 2018) that are generally difficult to achieve either due to too low resolution of

dating techniques (Daniels *et al.*, 2018; Englert *et al.*, 2020) or too limited in time and/or stratigraphic extent (Flood & Piper, 1997; Jobe *et al.*, 2015).

B Can an equilibrium profile model explain the observed architectural style changes?

The stratigraphic evolution of Complex 4 is intriguing since it reflects changes in channel morphodynamics that likely occur within a time-span of a few kyr (see *Time-duration of Complex 4 and its building block* section) and develops over a thickness that would render it difficult to resolve in subsurface seismic exploration. Unfortunately, full understanding of development of Complex 4 is hampered by the lack of constraints on the coeval slope profile and on how this evolved in response to sedimentation and/or tectonic deformation.

Stratigraphic transitions from erosional channel fills similar to those of the inception phase (see *Phase 1: Channel belt inception* section) to composite sheets with LAPs, such that of the middle part of Complex 4 (see *Phase 2: Channel belt meandering and blanketing by muddy sheets* section), have been documented elsewhere (Peakall *et al.*, 2000; Kneller, 2003; Babonneau *et al.*, 2010; Fildani *et al.*, 2013; Jobe *et al.*, 2015) and can be explained in an equilibrium profile perspective. In fact, establishment of Phase 2 is highly suggestive of a waxing of sediment supply that, following the flow parameter model of Kneller (2003), might have forced the channel to increase its sinuosity, resulting in widespread bend expansion and lateral accretion.

However, a simple equilibrium profile model would predict that, if in a later stage sediment input remained constant, the channel would rapidly reach a steady-state sinuosity and then aggrade (Peakall *et al.*, 2000). Such behaviour, widely documented and prone to kinematics modelling (Deptuck *et al.*, 2007; McHargue *et al.*, 2011; Covault *et al.*, 2016), reflects the inherent structure of turbidity currents in turbidite channels, whereby density stratification and flow super elevation promote significant overbank deposition and levee growth. Attainment of an equilibrium profile will result in a 'hockey stick' trajectory (*sensu* Jobe *et al.*, 2016) in which subsequent channel fills are initially laterally stacked and evolve stratigraphically into a

vertically stacked pattern. This 'hockey stick' architecture has been reported from numerous submarine channels (Peakall *et al.*, 2000; Fildani *et al.*, 2013; Jobe *et al.*, 2016; Englert *et al.*, 2020), suggesting that the equilibrium profile represents a main autocyclical control.

Complex 4 seems hard to fit into a 'hockey stick' model in that the establishment of its late aggradational phase (see *Phase 3: channel re-establishment, aggradation and abandonment* section) is preceded by a relatively prolonged time-span of reduced sediment input during which the preceding channel belt was blanketed by muddy sheets interpretable as retrogressive terminal lobes. Whether this reflected a reduction in run-off or augmented shelf sediment storage (for example, due to a relative sea-level rise) is unclear, but was likely accompanied with steepening of the channel profile up-dip of the study area. It can be thus argued that the late aggradational phase of Complex 4 resulted from a further increase in prevailing sediment discharge that, following Kneller (2003) model and similarly to comparable systems (Pirmez *et al.*, 2000; Samuel *et al.*, 2003; Hodgson *et al.*, 2011), might have promoted rapid degradation of the channel profile up-dip and contemporaneous aggradation in the study area.

Alternatively, a 'hockey stick' architecture for the upper part of Complex 4 could still be true if presence of a laterally accreted and extensive sandstone is postulated below the Plio-Quaternary covers to the west of the Zobzit river (Bernini *et al.*, 1994; Gelati *et al.*, 2000; Felletti *et al.*, 2020), sandwiched below the muddy terminal lobes and the late aggradation phase (see *Phase 3: channel re-establishment, aggradation and abandonment* section).

All in all, the depositional architecture of Complex 4 is unique and highlights how changes in sediment supply and flow properties at a range of temporal scales (McHargue *et al.*, 2011; Payros & Martínez-Braceras, 2014; Catuneanu, 2019, 2020; Marini *et al.*, 2020) can modulate the longer-term adjustment of submarine channels to a profile of equilibrium (Peakall *et al.*, 2000; Pirmez *et al.*, 2000; Samuel *et al.*, 2003; Jobe *et al.*, 2016) and result in highly intricate sedimentary heterogeneity.

A CONCLUSIONS

The up to *ca* 20 m thick channel-levee Complex 4 constitutes part of the Tachrift turbidite subunit (late Tortonian). It represents the sedimentary product of a slope sinuous channel that crossed the south-bounding slope of the Taza-Guercif Basin (north-east Morocco), evolving over time contemporaneously with deposition of hemipelagic marlstones. Physical correlation of 84 sedimentary logs spanning an outcrop belt *ca* 3.4 km long largely oblique to mean palaeoflow shows that Complex 4 is characterized by stratigraphic changes of architectural style which can be used to track the morphodynamic evolution of the parent channel and make inferences on likely control factors. Results are as follows:

- The elemental building blocks of the investigated architecture are single-storey channel fills and associated levees. These are sets of several event beds that can stack vertically with minor off-set ('cut-and-fill' storeys) or form largely sigmoidal laterally accretion packages (LAPs). These are interpreted to result from deposition in relatively straight erosional channels and sinuous meandering channels, respectively.
- The sandstone parts of subsequent single-storeys can be locally amalgamated but are more frequently separated from one another by heterolithic muddier intervals. The sandstone and the heterolithic components of single-storeys are interpreted to reflect waxing and waning-phases of sediment discharge, respectively.
- Storeys with a common migration pathways form larger units (storey-sets) characterized by aggradational versus laterally migrating trajectories.
- The spatial stacking of single-storeys and storey-sets reflect a range of processes, including channel bend expansion (swing), down-slope translation of channel bends (sweep), channel avulsion, and variable degree of channel (and levee) aggradation.
- Overall, the complex shows a three-fold stratigraphic evolution including: (i) a lowermost mud-prone interval with relatively small (a few hundred of metres across and metre-thick) and vertically stacked fills of erosional channels sided by muddy levees (Phase 1); (ii) a middle >1 km wide sandstone-rich unit made of LAPs, which becomes finer grain and less

amalgamated upward and passes into muddy sheets with intercalations of marly hemipelagites and small channel fills (Phase 2); and (iii) an uppermost package of vertically aggraded channel fills with variously directed LAPs and well-developed levees (Phase 3).

- Phase 1 is interpreted as the sedimentary record of a stage of channel inception, established when turbidity currents first reached the studied sector of the slope upon initial waxing of sediment discharge.
- Phase 2 records an interval of time when sinuosity increased as the channel adjusted its gradient to increasing sediment input, resulting is formation of an extensive laterally accreted unit. Phase 2 terminates with a progressive waning of sediment discharge that culminates in blanketing of the preceding channel belt by 'retrogressive' muddy lobes.
- Phase 3 heralds the establishment of a high accommodation regime in which levees aggrade contemporaneously with the channel prior to local deactivation of the complex.
- Based on magnetochronology from literature and lithological calibration from this work, the estimated time duration of this complex is of several thousand years.
- The documented stratigraphic evolution is unique and does not fit the simple 'hockey stick' architecture developed by numerous channel systems as they tend to an equilibrium profile.
- It is suggested here that changes in sediment supply and flow properties at a range of temporal scales can modulate the longer-term adjustment of submarine channels to a profile of equilibrium and result in the large variety of architectures documented to date.

A ACKNOWLEDGEMENTS

Financial support was provided by the University of Milan and 'Ministero dell'Università e della Ricerca' of Italy. The local Authorities of Douar Tachrift and Ras El Ksar are warmly thanked for providing access to outcrops and logistic support. Also, authors wish to thank Nicolò Bellin and Ahmed Zghida for helping during the field work and the Hachimi family in Douar Ras El Ksar for their hospitality. In addition, authors would like to thank editor and anonymous reviewers for helping by providing constructive comments on improving the manuscript.

A DATA AVAILABILITY STATEMENT

Research data are not shared.

A REFERENCES

Abreu, V., **Sullivan, M.**, **Pirmez, C.** and **Mohrig, D.** (2003) Lateral accretion packages (LAPs): An important reservoir element in deep water sinuous channels. *Mar. Pet. Geol.*, **20**, 631–648.

Arnott, R.W.C. and **Hand, B.M.** (1989) Bedforms, primary structures and grain fabric in the presence of suspended sediment rain. *J. Sediment. Res.*, **59**, 1062–1069.

Arnott, R.W.C., **Tilston, M.**, **Fraino, P.**, **Navarro, L.**, **Dumouchel, G.** and **Miklovich, N.** (2021) Laterally accreting sinuous channels and their deposits: The goldilocks of deep-water slope systems. *J. Sediment. Res.*, **91**, 451–463.

Babonneau, N., **Savoye, B.**, **Cremer, M.** and **Bez, M.** (2010) Sedimentary Architecture in Meanders of a Submarine Channel: Detailed Study of the Present Congo Turbidite Channel (Zaiango Project). *J. Sediment. Res.*, **80**, 852–866.

Beaubouef, R.T. (2004) Deep-water leveed-channel complexes of the Cerro Toro Formation, Upper Cretaceous, southern Chile. *Am. Assoc. Pet. Geol. Bull.*, **88**, 1471–1500.

Benzaquen, M. (1965) Etude stratigraphique préliminaire des formations du bassin de Guercif. Verlag nicht ermittelbar

Bernini, M., **Boccaletti, M.**, **El Mokhtari, J.**, **Gelati, R.**, **Moratti, G.** and **Papani, G.** (1994) Geologic-structural Map of the Taza-Guercif Neogene basin (North eastern Morocco). Scale 1: 50,000.

Bernini, M., **Boccaletti, M.**, **Gelati, R.**, **Moratti, G.**, **Papani, G.** and **Mokhtari, J. El** (1999) Tectonics and sedimentation in the Taza-Guercif Basin, northern Morocco: Implications for the Neogene evolution of the Rif-Middle Atlas Orogenic System. *J. Pet. Geol.*, **22**, 115–128.

Bernini, M., **Boccaletti, M.**, **Moratti, G.** and **Papani, G.** (2000) Structural development of the Taza-Guercif Basin as a constraint for the Middle Atlas Shear Zone tectonic evolution. *Mar. Pet. Geol.*, **17**, 391–408.

Bouma, A.H. (1962) Sedimentology of some flysch deposits.

Bridge, J.S. (2003) Rivers and floodplains. Forms, Processes and Sedimentary RecordBlackwell Science. 512 pp.

Camacho, H., **Busby, C.J.** and **Kneller, B.** (2002) A new depositional model for the classical turbidite locality at San Clemente State Beach, California. *Am. Assoc. Pet. Geol. Bull.*, **86**, 1543–1560.

Campbell, C. V (1967) Lamina, Laminaset, Bed and Bedsets. *Sedimentology*, **8**, 7–26.

Capella, W., **Barhoun, N.**, **Flecker, R.**, **Hilgen, F.J.**, **Kouwenhoven, T.**, **Matenco, L.C.**, **Sierro, F.J.**, **Tulbure, M.A.**, **Yousfi, M.Z.** and **Krijgsman, W.** (2018) Palaeogeographic evolution of the late Miocene Rifian Corridor (Morocco): Reconstructions from surface and subsurface data. *Earth-Science Rev.*, **180**, 37–59.

Capella, W., **Flecker, R.**, **Hernández-Molina, F.J.**, **Simon, D.**, **Meijer, P.T.**, **Rogerson, M.**, **Sierro, F.J.** and **Krijgsman, W.** (2019) Mediterranean isolation preconditioning the Earth System for late Miocene climate cooling. *Sci. Rep.*, **9**, 1–8.

Capella, W., **Matenco, L.**, **Dmitrieva, E.**, **Roest, W.M.J.**, **Hessels, S.**, **Hssain, M.**, **Chakor-Alami, A.**, **Sierro, F.J.** and **Krijgsman, W.** (2017) Thick-skinned tectonics closing the Rifian Corridor. *Tectonophysics*, **710**–**711**, 249–265.

Catuneanu, O. (2019) Scale in sequence stratigraphy. *Mar. Pet. Geol.*, **106**, 128–159.

Catuneanu, O. (2020) Sequence stratigraphy of deep-water systems. *Mar. Pet. Geol.*, **114**, 104–238.

Colletta, B. (1977) Evolution neotectonique de la partie meridionale du bassin de Guercif (Maroc Oriental). Université Scientifique et Mèdicale de Grenoble

Counts, J.W., **Amy, L.**, **Georgiopoulou, A.** and **Haughton, P.** (2021) A review of sand detachment in modern deep marine environments: Analogues for upslope stratigraphic traps. *Mar. Pet. Geol.*, **132**, 105184.

Covault, J.A., **Sylvester, Z.**, **Hubbard, S.M.**, **Jobe, Z.R.** and **Sech, R.P.** (2016) The Stratigraphic Record of Submarine-Channel Evolution. *Sediment. Rec.*, **14**, 4–11.

Covault, J.A., **Sylvester, Z.**, **Hudec, M.R.**, **Ceyhan, C.** and **Dunlap, D.** (2020) Submarine channels 'swept' downstream after bend cutoff in salt basins. *Depos. Rec.*, **6**, 259–272.

Cronin, B.T., **Hurst, A.**, **Celik, H.** and **Türkmen, I.** (2000) Superb exposure of a channel, levee and overbank complex in an ancient deep-water slope environment. *Sediment. Geol.*, **132**, 205–216.

Cullis, S., **Colombera, L.**, **Patacci, M.** and **McCaffrey, W.D.** (2018a) Hierarchical classifications of the sedimentary architecture of deep-marine depositional systems. *Earth-Science Rev.*, **179**, 38–71.

Cullis, S., **Colombera, L.**, **Patacci, M.** and **McCaffrey, W.D.** (2018b) Hierarchical classifications of the sedimentary architecture of deep-marine depositional systems. 38–71 pp.

Daniels, B.G., **Auchter, N.C.**, **Hubbard, S.M.**, **Romans, B.W.**, **Matthews, W.A.** and **Stright, L.** (2018) Timing of deep-water slope evolution constrained by large-n detrital and volcanic ash zircon geochronology, Cretaceous Magallanes Basin, Chile. *Bull. Geol. Soc. Am.*, **130**, 438–454.

de Lamotte, D.F., **Leturmy, P.**, **Missenard, Y.**, **Khomsi, S.**, **Ruiz, G.**, **Saddiqi, O.**, **Guillocheau, F.** and **Michard, A.** (2009) Mesozoic and Cenozoic vertical movements in the Atlas system (Algeria, Morocco, Tunisia): an overview. *Tectonophysics*, **475**, 9–28.

Deptuck, M.E., **Sylvester, Z.**, **Pirmez, C.** and **O'Byrne, C.** (2007) Migration-aggradation history and 3-D seismic geomorphology of submarine channels in the Pleistocene Benin-major Canyon, western Niger Delta slope. *Mar. Pet. Geol.*, **24**, 406–433.

Dykstra, M. and **Kneller, B.** (2009) Lateral accretion in a deep-marine channel complex: Implications for channellized flow processes in turbidity currents. *Sedimentology*, **56**, 1411–1432.

Elliott, T. (2000) Depositional architecture of a sand-rich, channelized turbidite system: the Upper Carboniferous Ross Sandstone Formation, western Ireland. In: *Deep-water reservoirs of the world: Gulf Coast Section Society for Sedimentary Geology, GCSSEPM Foundation Annual Bob F. Perkins Research Conference Proceedings*, 20, 342–373.

Englert, R.G., **Hubbard, S.M.**, **Matthews, W.A.**, **Coutts, D.S.** and **Covault, J.A.** (2020) The evolution of submarine slope-channel systems: Timing of incision, bypass, and aggradation in late cretaceous nanaimo group channel-system strata, British Columbia, Canada. *Geosphere*, **16**, 281–296.

Felletti, F., **Marini, M.**, **El Kati, I.** and **Tabyaoui, H.** (2020) The Tachrift channel-levee turbidite complexes (Tortonian) of the Taza-Guercif basin (South Rifian Corridor, NE Morocco). *J. Maps*, **16**, 902–917.

Fildani, A., **Hubbard, S.M.**, **Covault, J.A.**, **Maier, K.L.**, **Romans, B.W.**, **Traer, M.** and **Rowland, J.C.** (2013) Erosion at inception of deep-sea channels. *Mar. Pet. Geol.*, **41**, 48–61.

Flecker, R., **Krijgsman, W.**, **Capella, W.**, **de Castro Martíns, C.**, **Dmitrieva, E.**, **Mayser, J.P.**, **Marzocchi, A.**, **Modestou, S.**, **Ochoa, D.**, **Simon, D.**, **Tulbure, M.**, **van den Berg, B.**, **van der Schee, M.**, **de Lange, G.**, **Ellam, R.**, **Govers, R.**, **Gutjahr, M.**, **Hilgen, F.**, **Kouwenhoven, T.**, **Lofi, J.**, **Meijer, P.**, **Sierro, F.J.**, **Bachiri, N.**, **Barhoun, N.**, **Alami, A.C.**, **Chacon, B.**, **Flores, J.A.**, **Gregory, J.**, **Howard, J.**, **Lunt, D.**, **Ochoa, M.**, **Pancost, R.**, **Vincent, S.** and **Yousfi, M.Z.** (2015) Evolution of the Late Miocene Mediterranean–Atlantic gateways and their impact on regional and global environmental change. *Earth-Science Rev.*, **150**, 365–392.

Flood, R.D. and **Piper, D.J.W.** (1997) Amazon Fan sedimentation: the relationship to equatorial climate change, continental denudation, and sea-level fluctuations. In: *Proceedings-Ocean Drilling Program Scientific Results*, *National science foundation*, 653–675.

Fonnesu, M., **Palermo, D.**, **Galbiati, M.**, **Marchesini, M.**, **Bonamini, E.** and **Bendias, D.** (2020) A new world-class deep-water play-type, deposited by the syndepositional interaction of turbidity flows and bottom currents: The giant Eocene Coral Field in northern Mozambique. *Mar. Pet. Geol.*, **111**, 179–201.

Fraino, P.E., **William, R.** and **Navarro, L.** (2022) The influence of sediment supply on the stratigraphic evolution of an ancient passive margin deep-marine slope channel system, Windermere Supergroup, British Columbia, Canada. *J. Sediment. Res.*, **92**, 232–256.

Funk, J.E., **Slatt, R.M.** and **Pyles, D.R.** (2012) Quantification of static connectivity between deep-water channels and stratigraphically adjacent architectural elements using outcrop analogs. *Am. Assoc. Pet. Geol. Bull.*, **96**, 277–300.

García, M., **Ercilla, G.**, **Alonso, B.**, **Estrada, F.**, **Jané, G.**, **Mena, A.**, **Alvés, T.** and **Juan, C.** (2015) Deep-water turbidite systems: A review of their elements, sedimentary processes and depositional models. Their characteristics on the iberian margins. *Boletín Geológico y Min.*, **126**, 189–218.

Gardner, M.H. and **Borer, J.M.** (2000) Submarine channel architecture along a slope to basin profile, Brushy Canyon Formation, West Texas. *Bouma, A.H., Stone, C.G. (Eds.), Fine-Grained Turbid. Syst. AAPG Mem. 72 SEPM Spec. Publ. 68*, 195–214.

Gardner, M.H., **Borer, J.M.**, **Melick, J.J.**, **Mavilla, N.**, **Dechesne, M.** and **Wagerle, R.N.** (2003) Stratigraphic process-response model for submarine channels and related features from studies of Permian Brushy Canyon outcrops, West Texas. *Mar. Pet. Geol.*, **20**, 757–787.

Gelati, R., **Moratti, G.** and **Papani, G.** (2000) The Late Cenozoic sedimentary succession of the Taza-Guercif Basin, South Rifian Corridor, Morocco. *Mar. Pet. Geol.*, **17**, 373–390.

Georgiopoulou, A. and **Cartwright, J.A.** (2013) A critical test of the concept of submarine equilibrium profile. *Mar. Pet. Geol.*, **41**, 35–47.

Gong, C., **Steel, R.J.**, **Qi, K.** and **Wang, Y.** (2020) Deep-water channel morphologies, architectures, and population densities in relation to stacking trajectories and climate states. *Bull. Geol. Soc. Am.*, **133**, 287–306.

Hansen, L., **Callow, R.**, **Kane, I.** and **Kneller, B.** (2017) Differentiating submarine channel-related thin-bedded turbidite facies: Outcrop examples from the Rosario Formation, Mexico. *Sediment. Geol.*, **358**, 19–34.

Hansen, L.A.S., **Callow, R.H.T.**, **Kane, I.A.**, **Gamberi, F.**, **Rovere, M.**, **Cronin, B.T.** and **Kneller, B.C.** (2015) Genesis and character of thin-bedded turbidites associated with submarine channels. *Mar. Pet. Geol.*, **67**, 852–879.

Hiscott, R.N. (1978) Slope sediments - Encyclopedia of Sediments and Sedimentary Rocks. In: (Ed. G. V Middleton, M.J. Church, M. Coniglio, L.A. Hardie, and F.J. Longstaffe), *Springer Netherlands*, Dordrecht, 668–674.

Hodgson, D.M., **Di Celma, C.N.**, **Brunt, R.L.** and **Flint, S.S.** (2011) Submarine slope degradation and aggradation and the stratigraphic evolution of channel-levee systems. *J. Geol. Soc. London.*, **168**, 625–628.

Hubbard, S.M., **Covault, J.A.**, **Fildani, A.** and **Romans, B.W.** (2014) Sediment transfer and deposition in slope channels: Deciphering the record of enigmatic deep-sea processes from outcrop. *Geol. Soc. Am. Bull.*, **126**, 857–871.

Janbu, N.E., **Nemec, W.**, **Kirman, E.** and **Özaksoy, V.** (2007) Facies anatomy of a sand-rich channelized turbiditic system: the Eocene Kusuri Formation in the Sinop Basin, north-central Turkey. In: *Special Publication 38: International Association of Sedimentologists*, *International Association of Sedimentologists*, 38, 457–517.

Janocko, M., **Nemec, W.**, **Henriksen, S.** and **Warchoł, M.** (2013) The diversity of deep-water sinuous channel belts and slope valley-fill complexes. *Mar. Pet. Geol.*, **41**, 7–34.

Jobe, Z.R., **Howes, N.C.** and **Auchter, N.C.** (2016) Comparing submarine and fluvial channel kinematics: Implications for stratigraphic architecture. *Geology*, **44**, 931–934.

Jobe, Z.R., **Howes, N.C.**, **Straub, K.M.**, **Cai, D.**, **Deng, H.**, **Laugier, F.J.**, **Pettinga, L.A.** and **Shumaker, L.E.** (2020) Comparing Aggradation, Superelevation, and Avulsion Frequency of Submarine and Fluvial Channels. *Front. Earth Sci.*, **8**, 53.

Jobe, Z.R., **Sylvester, Z.**, **Parker, A.O.**, **Howes, N.**, **Slowey, N.** and **Pirmez, C.** (2015) Rapid adjustment of submarine channel architecture to changes in sediment supply. *J. Sediment. Res.*, **85**, 729–756.

Kane, I.A., **Catterall, V.**, **McCaffrey, W.D.** and **Martinsen, O.J.** (2010) Submarine channel response to intrabasinal tectonics: The influence of lateral tilt. *Am. Assoc. Pet. Geol. Bull.*, **94**, 189–219.

Kane, I.A. and **Clare, M.A.** (2019) Dispersion, accumulation, and the ultimate fate of microplastics in deep-marine environments: A review and future directions. Front Earth Sci. doi: 10.3389/feart.2019.00080

Kane, I.A. and **Hodgson, D.M.** (2011) Sedimentological criteria to differentiate submarine channel levee subenvironments: Exhumed examples from the Rosario Fm. (Upper Cretaceous) of Baja California, Mexico, and the Fort Brown Fm. (Permian), Karoo Basin, S. Africa. *Mar. Pet. Geol.*, **28**, 807–823.

Kane, I.A., **Mcgee, D.T.** and **Jobe, Z.R.** (2012) Halokinetic effects on submarine channel equilibrium profiles and implications for facies architecture: Conceptual model illustrated with a case study from magnolia field, Gulf of Mexico. *Geol. Soc. Spec. Publ.*, **363**, 289–302.

Kneller, B. (2003) The influence of flow parameters on turbidite slope channel architecture. *Mar. Pet. Geol.*, **20**, 901–910.

Kneller, B. and **McCaffrey, W.** (1999) Depositional effects of flow nonuniformity and stratification within turbidity currents approaching a bounding slope; deflection, reflection, and facies variation. *J. Sediment. Res.*, **69**, 980–991.

Kneller, B.C. and **Branney, M.J.** (1995) Sustained high-density turbidity currents and the deposition of thick massive sands. *Sedimentology*, **42**, 607–616.

Kolla, V. (2007) A review of sinuous channel avulsion patterns in some major deep-sea fans and factors controlling them. *Mar. Pet. Geol.*, **24**, 450–469.

Kolla, V., **Posamentier, H.W.** and **Wood, L.J.** (2007) Deep-water and fluvial sinuous channels—Characteristics, similarities and dissimilarities, and modes of formation. *Mar. Pet. Geol.*, **24**, 388–405.

Krijgsman, W. and **Langereis, C.G.** (2000) Magnetostratigraphy of the Zobzit and Koudiat Zarga sections (Taza-Guercif basin, Morocco): implications for the evolution of the Rifian Corridor. *Mar. Pet. Geol.*, **17**, 359–371.

Krijgsman, W., **Langereis, C.G.**, **Zachariasse, W.J.**, **Boccaletti, M.**, **Moratti, G.**, **Gelati, R.**, **Iaccarino, S.**, **Papani, G.** and **Villa, G.** (1999) Late Neogene evolution of the Taza–Guercif Basin (Rifian Corridor, Morocco) and implications for the Messinian salinity crisis. *Mar. Geol.*, **153**, 147–160.

Labourdette, R. and **Bez, M.** (2010) Element migration in turbidite systems: Random or systematic depositional processes? *Am. Assoc. Pet. Geol. Bull.*, **94**, 345–368.

Li, P., **Kneller, B.**, **Thompson, P.**, **Bozetti, G.** and **dos Santos, T.** (2018) Architectural and facies organisation of slope channel fills: Upper Cretaceous Rosario Formation, Baja California, Mexico. *Mar. Pet. Geol.*, **92**, 632–649.

Lowe, D.R. (1982) Sediment gravity flows; II, Depositional models with special reference to the deposits of high-density turbidity currents. *J. Sediment. Res.*, **52**, 279–297.

Lowe, D.R. (1988) Suspended-load fallout rate as an independent variable in the analysis of current structures. *Sedimentology*, **35**, 765–776.

Marini, M., **Maron, M.**, **Petrizzo, M.R.**, **Felletti, F.** and **Muttoni, G.** (2020) Magnetochronology applied to assess tempo of turbidite deposition: A case study of ponded sheet-like turbidites from the lower Miocene of the northern Apennines (Italy). *Sediment. Geol.*, **403**, 105654.

McHargue, T., **Pyrcz, M.J.**, **Sullivan, M.D.**, **Clark, J.D.**, **Fildani, A.**, **Romans, B.W.**, **Covault, J.A.**, **Levy, M.**, **Posamentier, H.W.** and **Drinkwater, N.J.** (2011) Architecture of turbidite channel systems on the continental slope: Patterns and predictions. *Mar. Pet. Geol.*, **28**, 728–743.

Mulder, T. and **Alexander, J.** (2001) The physical character of subaqueous sedimentary density flow and their deposits. *Sedimentology*, **48**, 269–299.

Mutti, E. (1992) Turbidite sandstones. *Agip - Ist. di Geol. Univ. di Parma, Italy, Spec. Publ.*, 275.

Navarro, L., **Khan, Z.** and **Arnott, R.W.C.** (2007) Depositional Architecture and Evolution of a Deep-marine Channel-levee Complex: Isaac Formation (Windermere Supergroup), Southern Canadian Cordillera. 22 pp.

Ogg, J.G. (2020) Geomagnetic polarity time scale. In: *Geologic time scale 2020*, *Elsevier*, 159–192.

Park, Y., **Yoo, D.**, **Kang, N.**, **Yi, B.** and **Kim, B.** (2021) Tectonic control on mass-transport deposit and canyon-fed fan system in the Ulleung Basin, East Sea (Sea of Japan). *Basin Res.*, **33**, 991–1016.

Patacci, M. (2016) A high-precision Jacob's staff with improved spatial accuracy and laser sighting capability. *Sediment. Geol.*, **335**, 66–69.

Payros, A. and **Martínez-Braceras, N.** (2014) Orbital forcing in turbidite accumulation during the Eocene greenhouse interval. *Sedimentology*, **61**, 1411–1432.

Peakall, J., **McCaffrey, B.** and **Kneller, B.** (2000) A process model for the evolution, morphology, and architecture of sinuous submarine channels. *J. Sediment. Res.*, **70**, 434–448.

Peakall, J. and **Sumner, E.J.** (2015) Submarine channel flow processes and deposits: A process-product perspective. *Geomorphology*, **244**, 95–120.

Pettingill, H.S. and **Weimer, P.** (2002) World-Wide Deepwater Exploration and Production: Past, Present and Future. *Proc. Annu. Offshore Technol. Conf.*, **21**, 371–376.

Pickering, K., **Stow, D.**, **Watson, M.** and **Hiscott, R.** (1986) Deep-water facies, processes and models: a review and classification scheme for modern and ancient sediments. *Earth Sci. Rev.*, **23**, 75–174.

Pickering, K.T. and **Cantalejo, B.** (2015) Deep-marine environments of the middle Eocene upper Hecho Group, Spanish Pyrenees: Introduction. *Earth-Science Rev.*, **144**, 1–9.

Picot, M., **Droz, L.**, **Marsset, T.**, **Dennielou, B.** and **Bez, M.** (2016) Controls on turbidite sedimentation: Insights from a quantitative approach of submarine channel and lobe architecture (Late Quaternary Congo Fan). *Mar. Pet. Geol.*, **72**, 423–446.

Pirmez, C., **Beaubouef, R.T.**, **Friedmann, S.J.**, **Mohrig, D.C.**, **Weimer, P.**, **Slatt, R.M.**, **Coleman, J.**, **Rosen, N.C.**, **Nelson, H.** and **Bouma, A.H.** (2000) Equilibrium profile and baselevel in submarine channels: examples from Late Pleistocene systems and implications for the architecture of deepwater reservoirs. In: *Global deep-water reservoirs: Gulf Coast Section SEPM Foundation 20th Annual Bob F. Perkins Research Conference*, 782–805.

Plink-Björklund, P. and **Steel, R.J.** (2004) Initiation of turbidity currents: Outcrop evidence for Eocene hyperpycnal flow turbidites. *Sediment. Geol.*, **165**, 29–52.

Posamentier, H.W. and **Kolla, V.** (2003) Seismic geomorphology and stratigraphy of depositional elements in deep-water settings. *J. Sediment. Res.*, **73**, 367–388.

Pratt, J.R., **Barbeau Jr, D.L.**, **Izykowski, T.M.**, **Garver, J.I.** and **Emran, A.** (2016) Sedimentary provenance of the Taza-Guercif Basin, South Rifean Corridor, Morocco: Implications for basin emergence. *Geosphere*, **12**, 221–236.

Pyles, D.R., **Tomasso, M.** and **Jennette, D.C.** (2012) Flow processes and sedimentation associated with erosion and filling of sinuous submarine channels. *Geology*, **40**, 143–146.

Qin, Y. (2017) Geological controls on the evolution of submarine channels in the Espírito Santo Basin , SE Brazil. Cardiff University

Reimchen, A.P., **Hubbard, S.M.**, **Stright, L.** and **Romans, B.W.** (2016a) Using sea-floor morphometrics to constrain stratigraphic models of sinuous submarine channel systems. *Mar. Pet. Geol.*, **77**, 92–115.

Reimchen, A.P., **Hubbard, S.M.**, **Stright, L.** and **Romans, B.W.** (2016b) Using sea-floor morphometrics to constrain stratigraphic models of sinuous submarine channel

systems. *Mar. Pet. Geol.*, **77**, 92–115.

Samuel, A., **Kneller, B.**, **Raslan, S.**, **Sharp, A.** and **Parsons, C.** (2003) Prolific deep-marine slope channels of the Nile Delta, Egypt. *Am. Assoc. Pet. Geol. Bull.*, **87**, 541–560.

Sani, F., **Zizi, M.** and **Bally, A.W.** (2000) The Neogene–Quaternary evolution of the Guercif Basin (Morocco) reconstructed from seismic line interpretation. *Mar. Pet. Geol.*, **17**, 343–357.

Sprague, A.R.G., **Garfield, T.R.**, **Goulding, F.J.**, **Beaubouef, R.T.**, **Sullivan, M.D.**, **Rossen, C.**, **Campion, K.M.**, **Sickafoose, D.K.**, **Abreu, V.**, **Schellpeper, M.E.**, **Jensen, G.N.**, **Jennette, D.C.**, **Pirmez, C.**, **Dixon, B.T.**, **Ying, D.**, **Ardill, J.**, **Mohrig, D.C.**, **Porter, M.L.**, **Farrell, M.E.** and **Mellere, D.** (2005) Integrated slope channel depositional models: the key to successful prediction of reservoir presence and quality in offshore West Africa.

Stevenson, C.J., **Jackson, C.A.L.**, **Hodgson, D.M.**, **Hubbard, S.M.** and **Eggenhuisen, J.T.** (2015) Deep-water sediment bypass. *J. Sediment. Res.*, **85**, 1058–1081.

Sylvester, Z., **Pirmez, C.** and **Cantelli, A.** (2011) A model of submarine channel-levee evolution based on channel trajectories: Implications for stratigraphic architecture. *Mar. Pet. Geol.*, **28**, 716–727.

Tek, D.E., **McArthur, A.D.**, **Poyatos-Moré, M.**, **Colombera, L.**, **Patacci, M.**, **Craven, B.** and **McCaffrey, W.D.** (2021) Relating seafloor geomorphology to subsurface architecture: How mass-transport deposits and knickpoint-zones build the stratigraphy of the deep-water Hikurangi Channel. *Sedimentology*, **68**, 3141–3190.

Torres Carbonell, P.J. and **Olivero, E.B.** (2019) Tectonic control on the evolution of depositional systems in a fossil, marine foreland basin: Example from the SE Austral Basin, Tierra del Fuego, Argentina. *Mar. Pet. Geol.*, **104**, 40–60.

Watson, S.J., **Mountjoy, J.J.** and **Crutchley, G.J.** (2020) Tectonic and geomorphic controls on the distribution of submarine landslides across active and passive margins, eastern New Zealand. *Geol. Soc. London, Spec. Publ.*, **500**, 477–494.

Weimer, P. (2000) Deep-Water Reservoirs of the World: 20th Annual. *Society of Economic Paleontologists and Mineralogists*.

Weimer, P. and **Pettingill, H.S.** (2007) Deep-water exploration and production: A global overview. *T. Nilsen, R. D. Shew, G. S. Steffens, J. Studlick, eds., Atlas Deep. outcrops world AAPG Stud. Geol.*, **56**, 29.

Wynn, R.B., **Cronin, B.T.** and **Peakall, J.** (2007) Sinuous deep-water channels: Genesis, geometry and architecture. *Mar. Pet. Geol.*, **24**, 341–387.

FIGURE AND TABLE CAPTIONS

Fig. 1. Geological sketch map of northern Morocco illustrating key structural elements and main terrains and Cenozoic basins (modified after Hafid *et al.*, 2006).

Fig. 2. (A) Schematic geological map of the Taza-Guercif basin (modified, after Felletti *et al.*, 2020). (B) Fence diagram showing the stratigraphic relationships between the component units of the sedimentary fill of the Taza-Guercif basin (modified, after Gelati *et al.*, 2000). (C) Stratigraphy of the Zobzit section with magnetostratigraphy (left-hand side), palaeobathymetry (left-hand side) and numbers identifying the channel-levee complexes of Felletti *et al.* (*2020)* (modified, after Krijgsman *et al.*, 1999).

Fig. 3. Simplified geological map showing location of outcrops of Complex 4, sedimentary logs and correlation panels discussed in the text (modified after Felletti *et al.*, 2020).

Fig. 4. Panoramic views of the lower and middle parts of Complex 4 in the central outcrop (see Figs 4 and 6 for location). (A) View orthogonal to mean palaeoflow (flow is away from the viewer) of the vertically stacked single-storey channel fills 1 to 5 and storey-sets A and B. (B) Channel fills storey-sets A to D make lateral transition to levee deposits to the right. (C) Oblique view showing the large-scale spatial stacking of the constituent storey-sets of the middle part of Complex 4. Note the interlayering of sandier and more amalgamated deposits and heterolithic intervals interpreted as waning-phase deposits (see Fig. 7B-b). (D) Detail showing the laterally accreted character of the channel fills (numbers identify single-storey channel fills) making the middle part of Complex 4 and the erosional contact of storey-set C onto storey-sets A and B (see *Results* section for details).

Fig. 5. Panoramic views orthogonal to mean palaeoflow (mean palaeoflow is away from the viewer) of the upper part of Complex 4 in the northern (A) and (B) and the southern (C) outcrops (see Figs 4 and 6 for location). (A) Eastward transition from sand-prone channel fills into heterolithics interpreted as levee deposits. (B) Storey-sets F–I in the north-westernmost outcrop of the Complex 4. (C) The channelized erosion characterising the southern outcrop.

Fig. 6. Large-scale correlation panel (see Fig. 3 for location) illustrating the stratigraphy and main facies associations of Complex 4. The panel is largely oblique to the mean palaeoflow (flow is away from the reader and towards the left; see inset rose diagram). Numbers and letters identify the single-storeys and storey-sets discussed in the *Channel fill* section.

Fig. 7. (A) Hierarchical classification (modified, after Sprague *et al.*, 2005, and Pickering & Cantalejo, 2015) for channelized deposits and bed thickness classification (after Campbell, 1967) used in this work. (B) Nomenclature used in this work to identify different parts of the channel fill of 'cut-and-fill' (top) versus meandering (bottom) channels.

Fig. 8. Medium to coarse-grained facies F1 to F3. (A) Massive sandstones with basal mud-chips (facies F1). The marker for scale is 1 cm wide. (B) Massive very coarse to medium-grained sandstones with centimetre-sized mud-chips (facies F1). The compass for scale is 6 cm wide. (C) Basal massive sandstones interval characterized by traction carpets (*mtc*) evolving upward into a horizontal plane-parallel laminated (*hpp*) top (facies F1). (D) Cross-stratified sandstones (*x-strat*) in facies F2. The pencil for scale is 10 cm long. (E) Low- angle cross-laminated sandstones with mud-clast basal lag (facies F2). (F) Horizontal plane-parallel laminated sandstones sharply overlain by a very thin cross-laminated (*x-lam*) top in facies F3.

Fig. 9. Fine-grained and chaotic, deformed facies F4 to F6. Different proportions of thin-bedded fine-grained sandstone, mudstones and subordinately marlstones form mud-prone (A) and sand-prone (B) intervals (facies F5 and F4, respectively). The marker for scale is 5 cm long. (C) Structureless siliciclastic turbidite mudstones and marlstones of facies F5, intercalated with rare very thin turbidite sandstone beds. (D) A detail of a carbonate concretion within mudstones of facies F5. (E) Massive conglomerates of facies F6 sit above the deep erosion documented in the southernmost sector (see Fig. 6C for location). (F) Detail showing the well-rounded carbonate clasts making the conglomerate of facies F6. The hammer for scale is 25 cm long.

Fig. 10. Correlation panel of the lower and middle parts of Complex 4 (see inset map and Fig. 3 for location and orientation). The panel is largely oblique to mean palaeoflow (flow is away from the viewer and towards the left).

Fig. 11. (A) Detail of Fig. 10 showing the internal organization and spatial stacking of the laterally accreted packages (LAPs) of single-storeys 8 to 11. Top-sets, middle-sets and toe-sets identify different portions of LAPs as detailed in Fig. 7B-b. (B) The beautifully exposed LAP of single-storey 10. Note the sigmoidal shape of component strata and how subsequent beds stack laterally towards the south-east. (C) Eastward accretion of subsequent storeys 7 to 11. Note how the waning-phase heterolithic deposits of storey 9 terminating with onlap geometry (white arrows) onto the underlaying LAP.

Fig. 12. (A) Strike-section panoramic view (mean palaoflow is away from the viewer) showing the contrasting direction of accrection of storey-set F and storey-set I of the upper Complex 4 (see Fig. 6 for loacation). (B) Oblique panoramic view (mean palaeoflow is away from the viewer and towards the right) showing the convex upward lensoidal shape of LAPs of storey-

sets F and G. (C) Srike-section panoramic view showing the superimposition of muddy thin-bedded turbidites interpeted as 'retrogressive' muddy lobes (see *Muddy sheets* section) onto storey-set E.

Fig. 13. Correlation panel of the upper Complex 4 (see inset map and Fig. 3 for location and orientation). Note how the levee deposits of storey-sets F to I are intercalated with relatively sandier bedsets interpreted as crevasse splay deposits (see *Levee deposits* section).

Fig. 14. Correlation panel of the upper Complex 4 from the northernmost outcrop (see inset map and Fig. 3 and for location and orientation). Note the lateral continuity of storey-sets and the confinement by correlative thin-bedded levees.

Fig. 15. Block diagram of showing the evolution of the aggradational upper part of Complex 4 (storey-sets F and I). Note how LAPs of storey-sets F to G and storey-set I show opposite direction of accretion as a result of meander downstream translation and the effect of compaction (right-hand side) the in older storey-sets makes locally difficult to tell original geometry and accretion direction.

Fig. 16. Evolutionary phases of Complex 4 (see *Large-scale architecture* and *Stratigraphic evolution of Complex 4* sections for explanation). The relative position of outcrops and logs was restored assuming a slope angle of 0.2° at time of deposition.

Fig. 17. Sketch map illustrating the inferred evolution of Complex 4 with location of correlation panels, palaeocurrents, and direction of accretion of lateral accretion packages (LAPs) used as constraints for interpretation.

Table 1. Summary of the sedimentary facies recognized within the channel-levee Complex 4.

Table 2. Maximum observed thickness and width for both single-storeys (above) and storey-sets. In bold, measurements and aspect ratios of fully exposed single-storey channel fills that are not cut by subsequent erosion.

Facies	Lithology	Sedimentological characteristics	Process interpretation
F1	Sandstones with a basal massive division	Coarse/medium to fine-grained, well to medium sorted, 15–100 cm thick beds. Structureless or with traction carpets, horizontal planar parallel lamination, ripple cross-lamination. Small mud clasts may be present close to base or scattered with bed	High-density turbidity currents. High suspended-load fallout rates, flow deceleration and bypass (Stevenson *et al*., 2015)
F2	Cross-stratified sandstones	Very coarse to medium/fine-grained, well to medium sorted, 10–100 cm thick beds. Trough-cross to cross-lamination, low-angle cross-lamination, ripple cross-lamination, horizontal plane-parallel lamination, traction carpets. Sometimes wavy top due to ripple-marks crests or bioturbation	2D or 3D dune formation underneath waning high-density turbidity currents (Lowe, 1982, 1988; Arnott & Hand, 1989)
F3	Planar parallel-laminated sandstones	Medium to fine-grained, well sorted, 15–100 cm thick beds. Horizontal plane-parallel lamination passing upward to ripple cross-lamination. Bioturbated top	Waning flow deposition. Partial bypass of sediment load (Lowe, 1988; Mulder & Alexander, 2001)
F4	Thin-bedded bioturbated sandstones	Fine to very fine-grained, medium sorted, 1–15 cm thick beds. Ripple-cross lamination, or water-escape structures. Intensely bioturbated	Waning low-density turbidity current deposition (Bouma, 1962; Pickering *et al*., 1986; Mulder & Alexander, 2001)
F5	Mudstones and marlstones	Clay to coarse silt, 0.5 to 200 cm thick. Structureless or weakly laminated. It may include structureless hemipelagic marlstone	Turbiditic and hemipelagic fall-out deposition (Mutti, 1992)
F6	Chaotic, deformed deposits	Clay to fine-grained sand with scattered centimetre to decimetre-thick sandstones blocks, or slumped marlstones, 20–500 cm thick	Debris flows, mass wasting, levee failure (Lowe, 1982; Picot *et al*., 2016; Qin, 2017; Counts *et al*., 2021)

Table 1. Summary of the sedimentary facies recognized within the channel-levee Complex 4.

	ID	Maximum observed thickness (m)	Maximum observed width (m)	Aspect ratio	Internal structure
Single-storey channel fills	1	**1.07**	**201**	**187**	Plane-parallel horizontal to sub-horizontal stratification
	2	**0.63**	**413**	**651**	
	3	**0.39**	**433**	**1101**	
	4	**0.86**	**447**	**520**	
	5	**0.85**	**375**	**440**	
	6	1.20	512	428	Laterally accreted bedsets
	7	1.09	444	409	
	8	1.32	432	327	Laterally accreted bedsets
	9	0.95	390	409	
	10	1.10	411	372	Laterally accreted bedsets
	11	2.14	387	181	
	12	0.68	441	648	–
	13	0.57	348	608	Laterally accreted bedsets
	14	1.05	216	206	
	15	0.72	174	240	
	16	**2.54**	**436**	**172**	Laterally accreted bedsets
	17	**2.84**	**447**	**157**	
	18	**0.85**	**554**	**648**	Laterally accreted bedsets
	19	**1.30**	**547**	**419**	
	20	**0.99**	**312**	**316**	Laterally accreted bedsets
	21	**0.84**	**448**	**531**	
	22	**0.74**	**300**	**408**	
	23	**2.44**	**472**	**194**	

	ID	Maximum observed thickness (m)	Maximum observed width (m)	Aspect ratio	Component storeys
Storey-sets	Δ	N/A	N/A	N/A	Not distinguished
	θ	3.50	450	128	2 to 5
	A	1.90	502	264	6 and 7
	B	1.77	429	242	8 and 9
	C	3.07	393	118	Not distinguished
	D	1.98	460	232	10 and 11
	E	1.78	524	294	Not distinguished
	F	2.04	851	417	13 to 15
	G	3.88	80	209	16 and 17
	H	1.65	641	387	18 and 19
	I	3.47	566	163	19 to 22

Table 2. Maximum observed thickness and width for both single-storeys (above) and storey-sets. In bold, measurements and aspect ratios of fully exposed single-storey channel fills that are not cut by subsequent erosion.

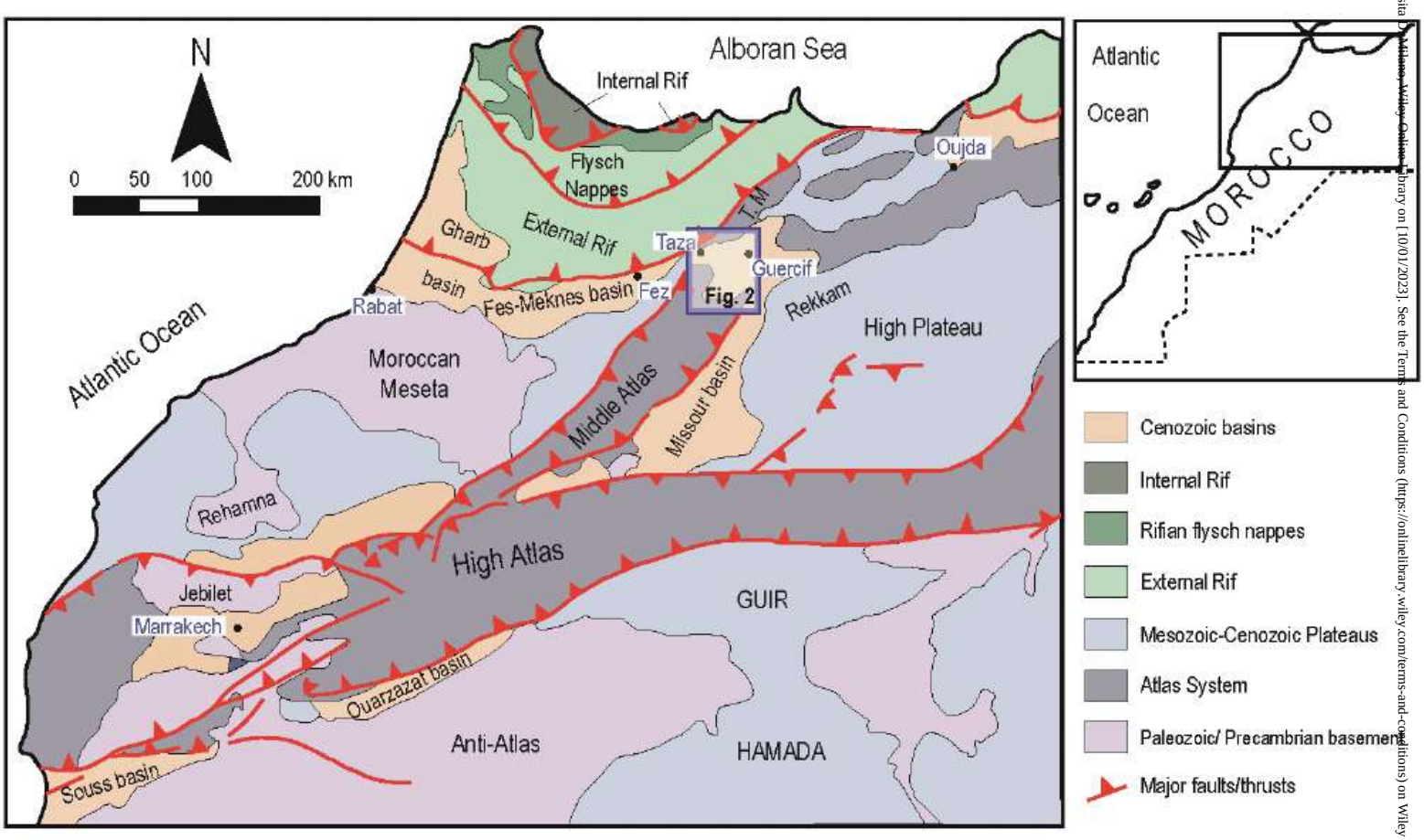

SED_13070_FIG1.tif

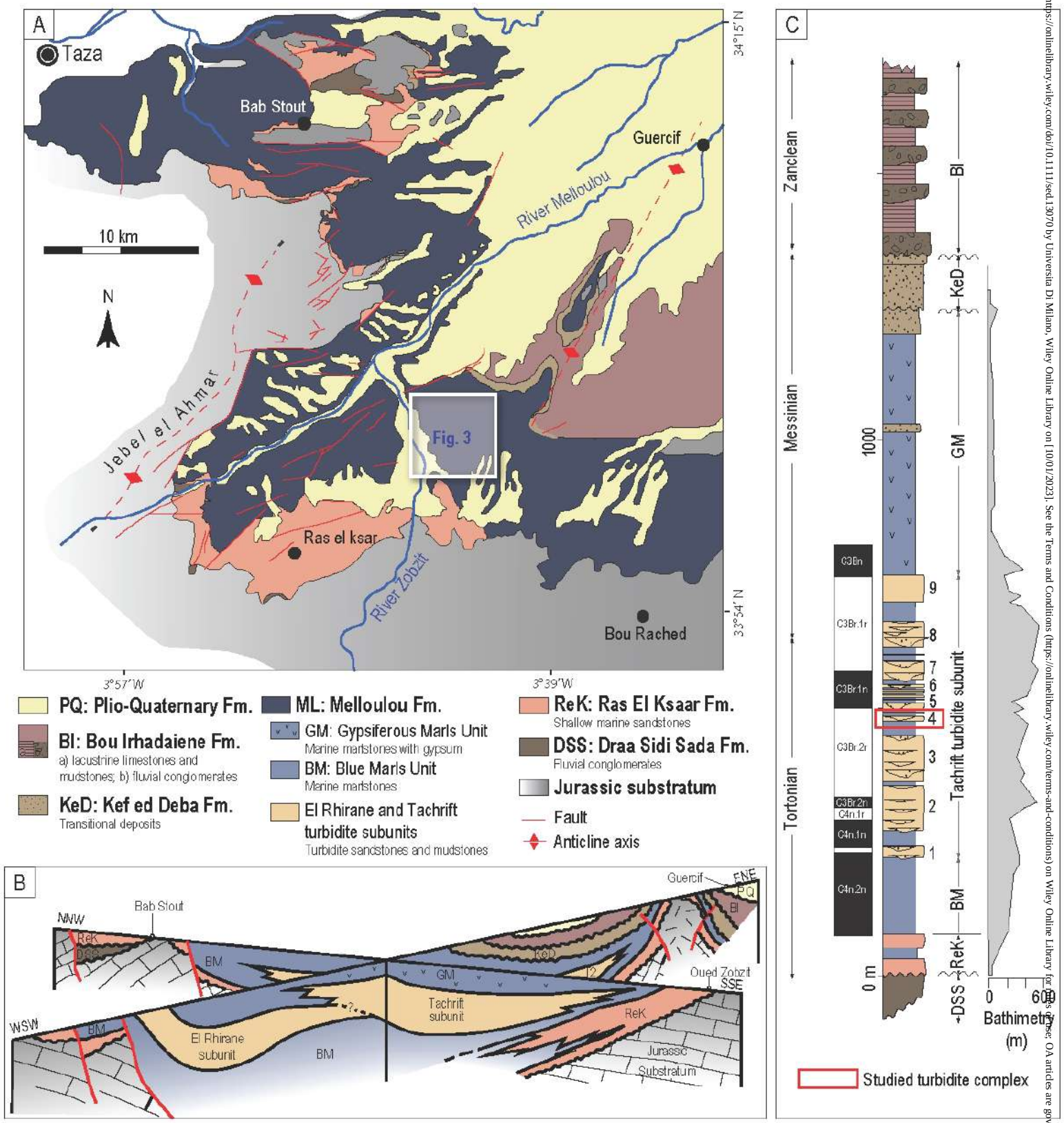

SED_13070_FIG2.tif

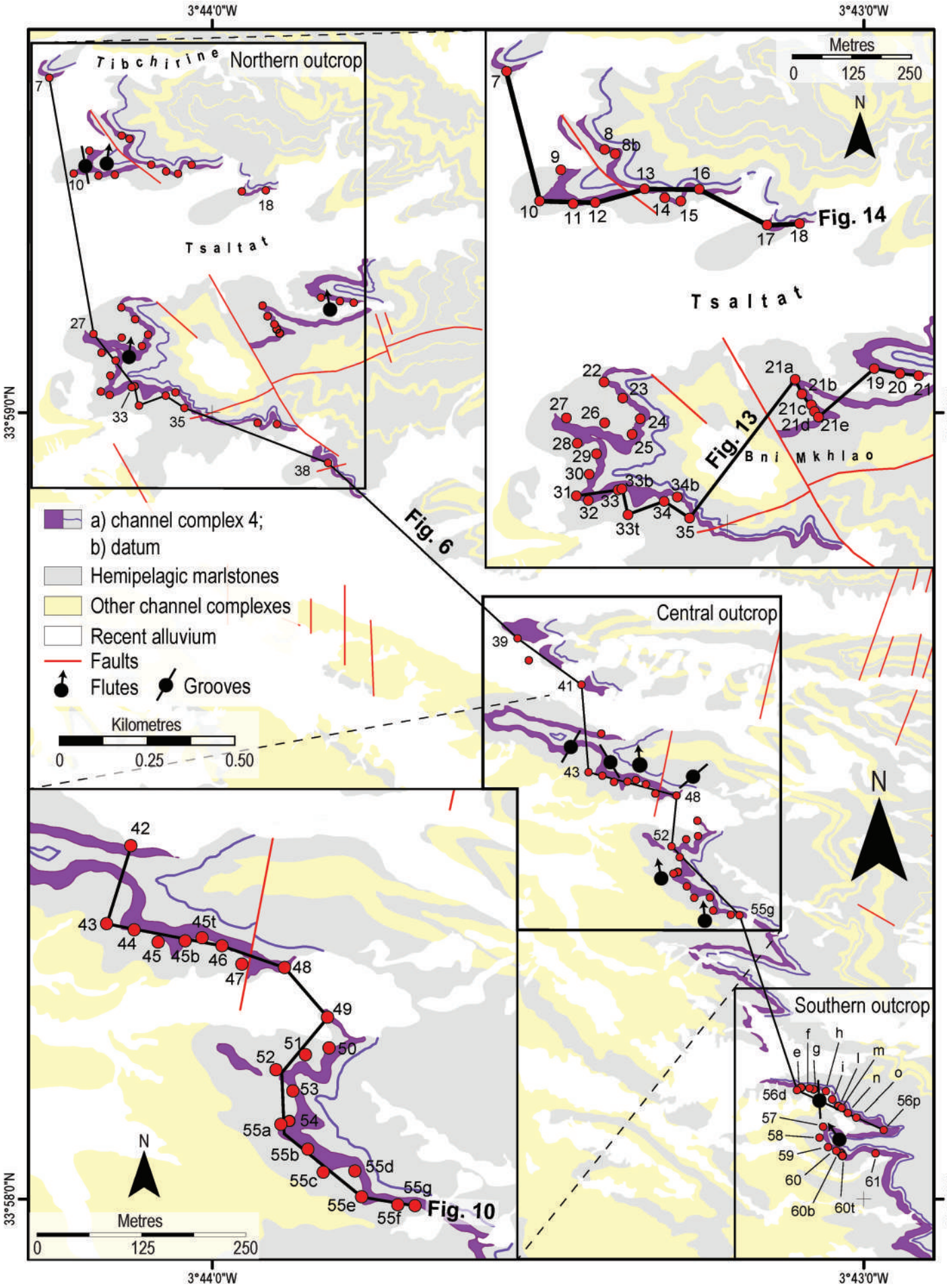

SED_13070_FIG3.tif

SED_13070_fig4_revSR_vert.tif

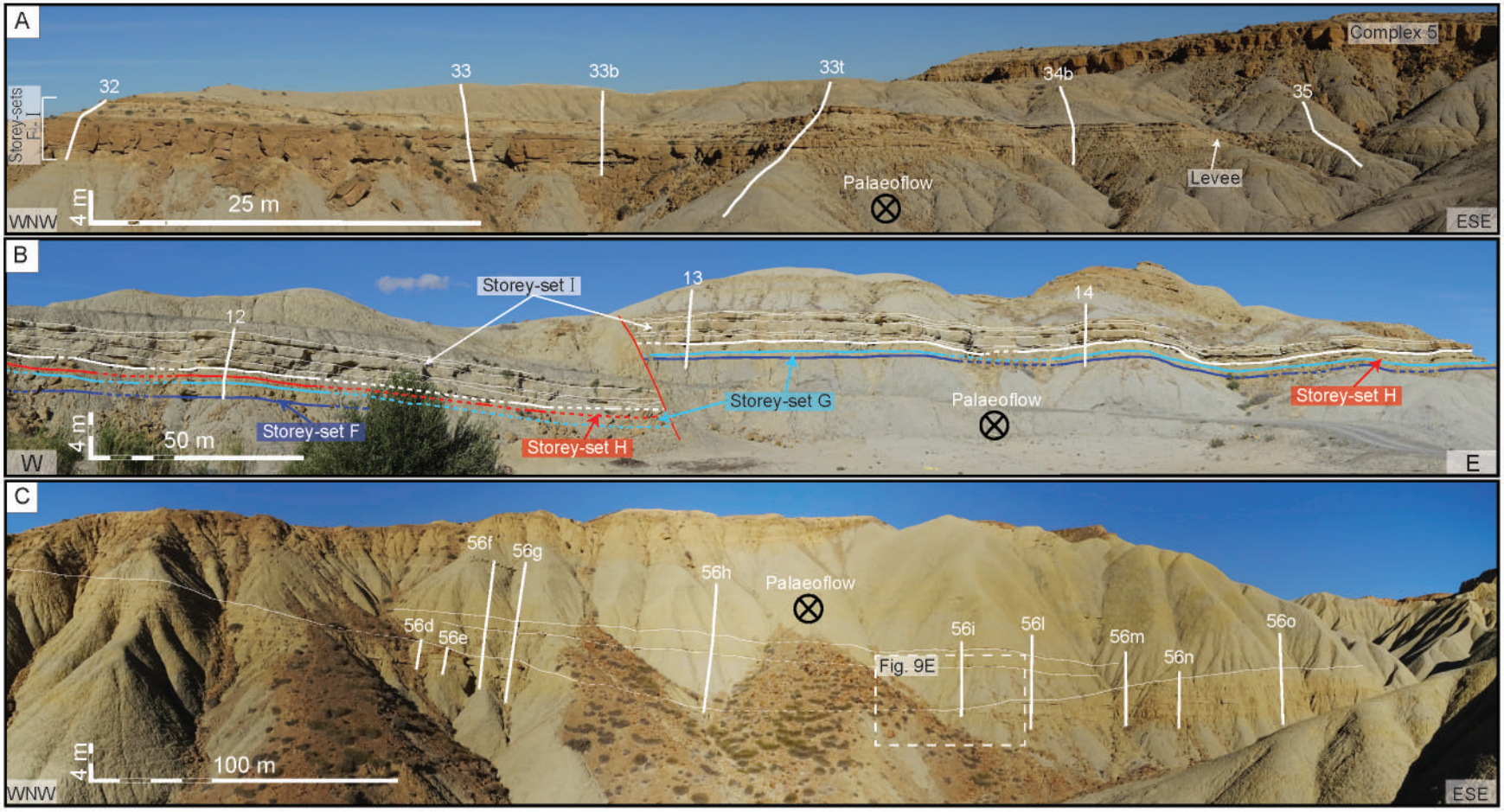

SED_13070_fig5_revSR.tiff

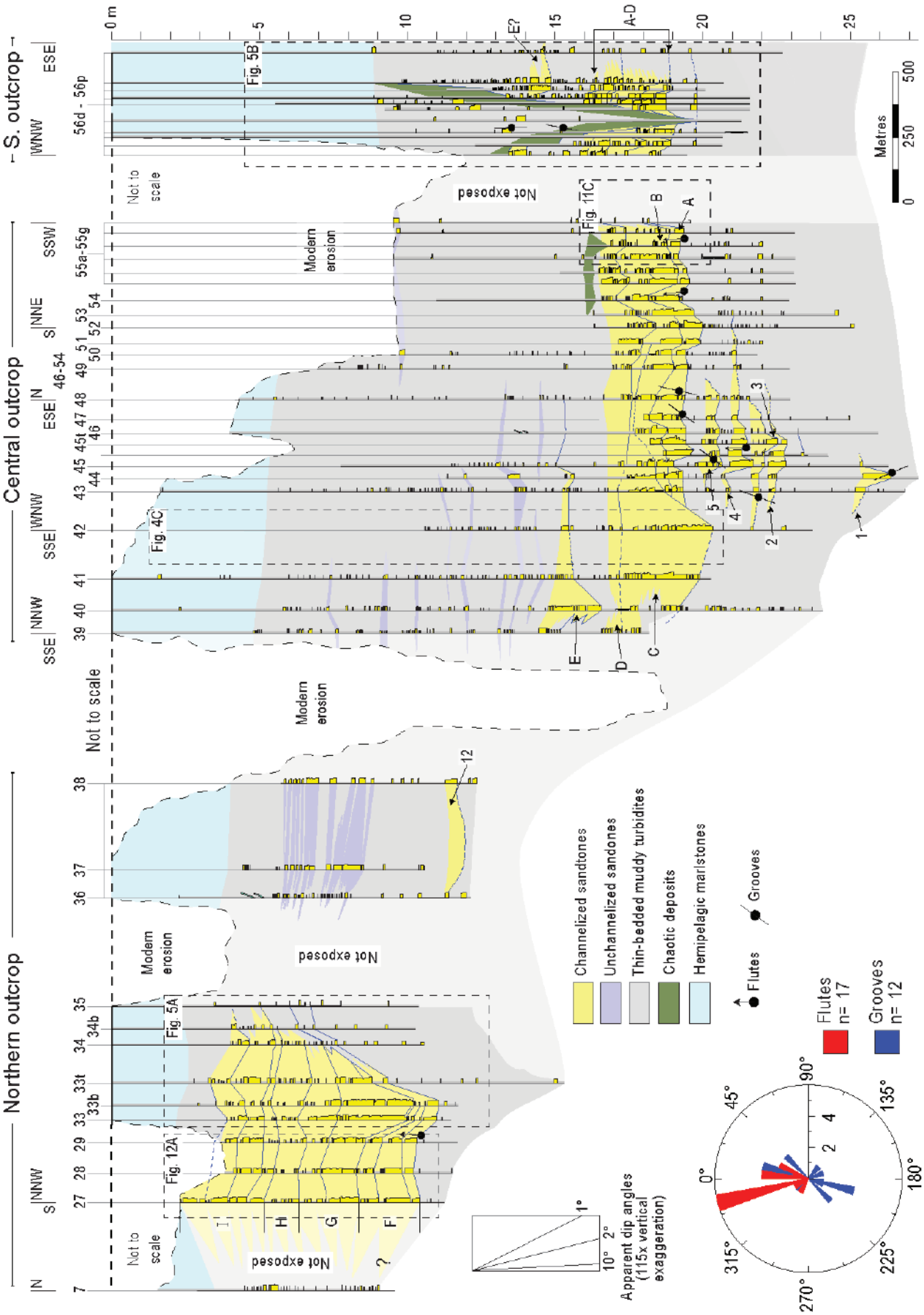

SED_13070_fig6_revSR.tiff

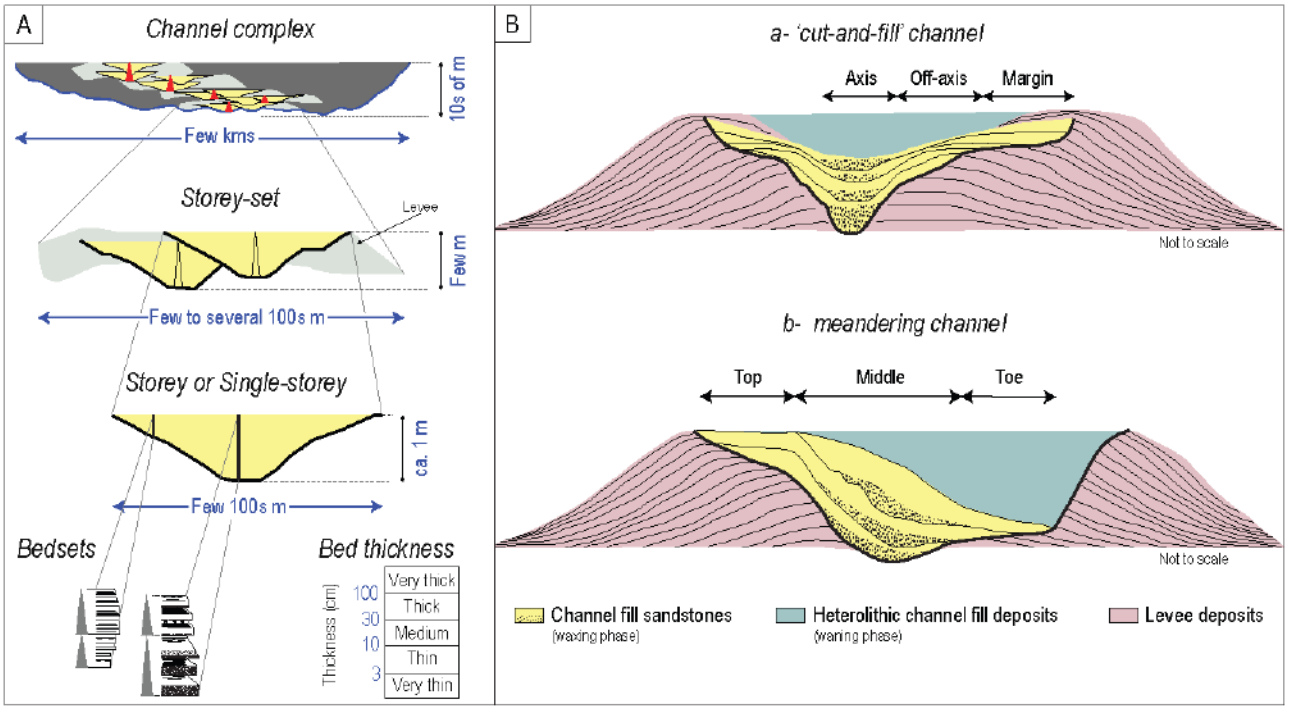

SED_13070_FIG7.tif

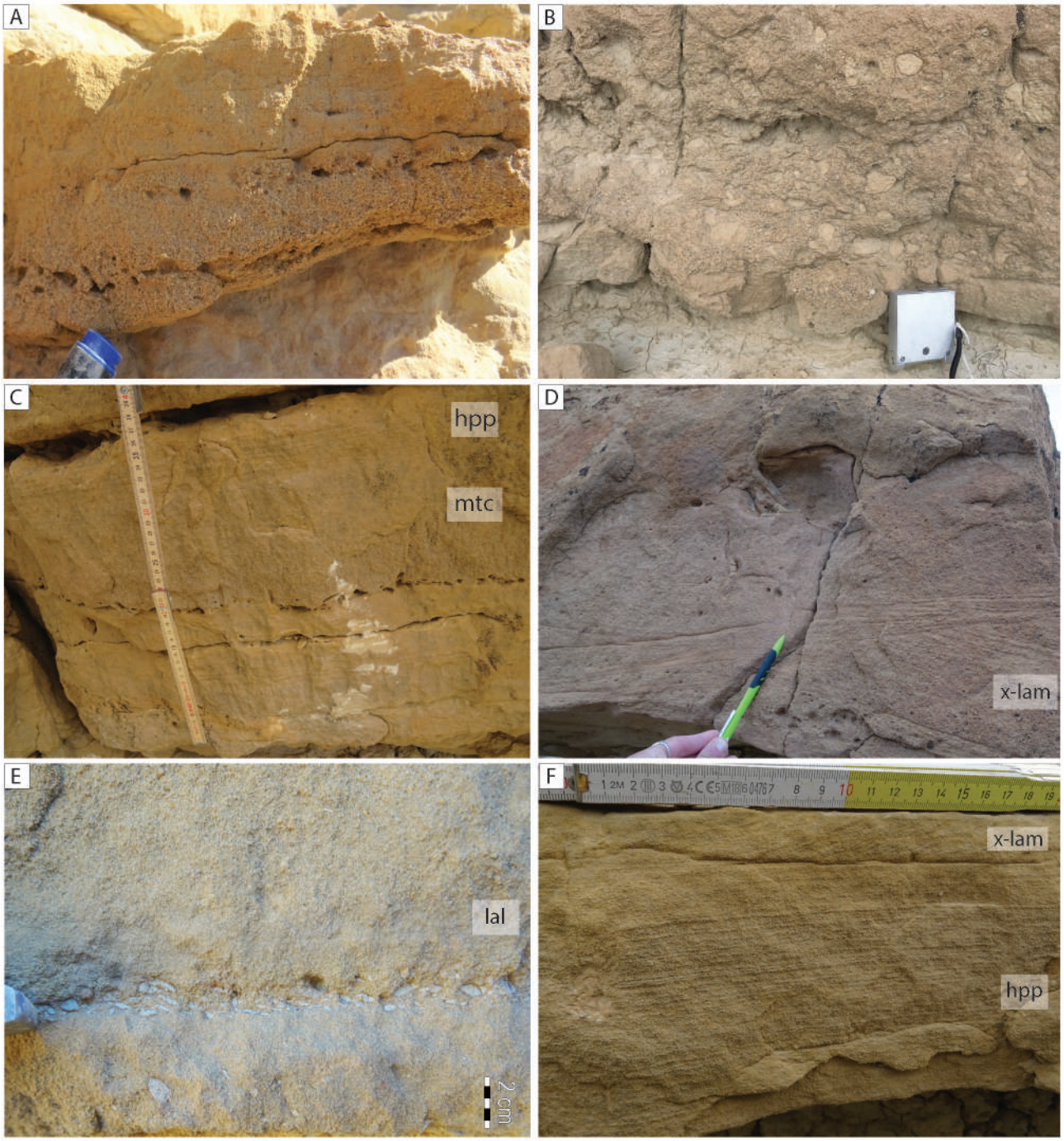

SED_13070_FIG8.tif

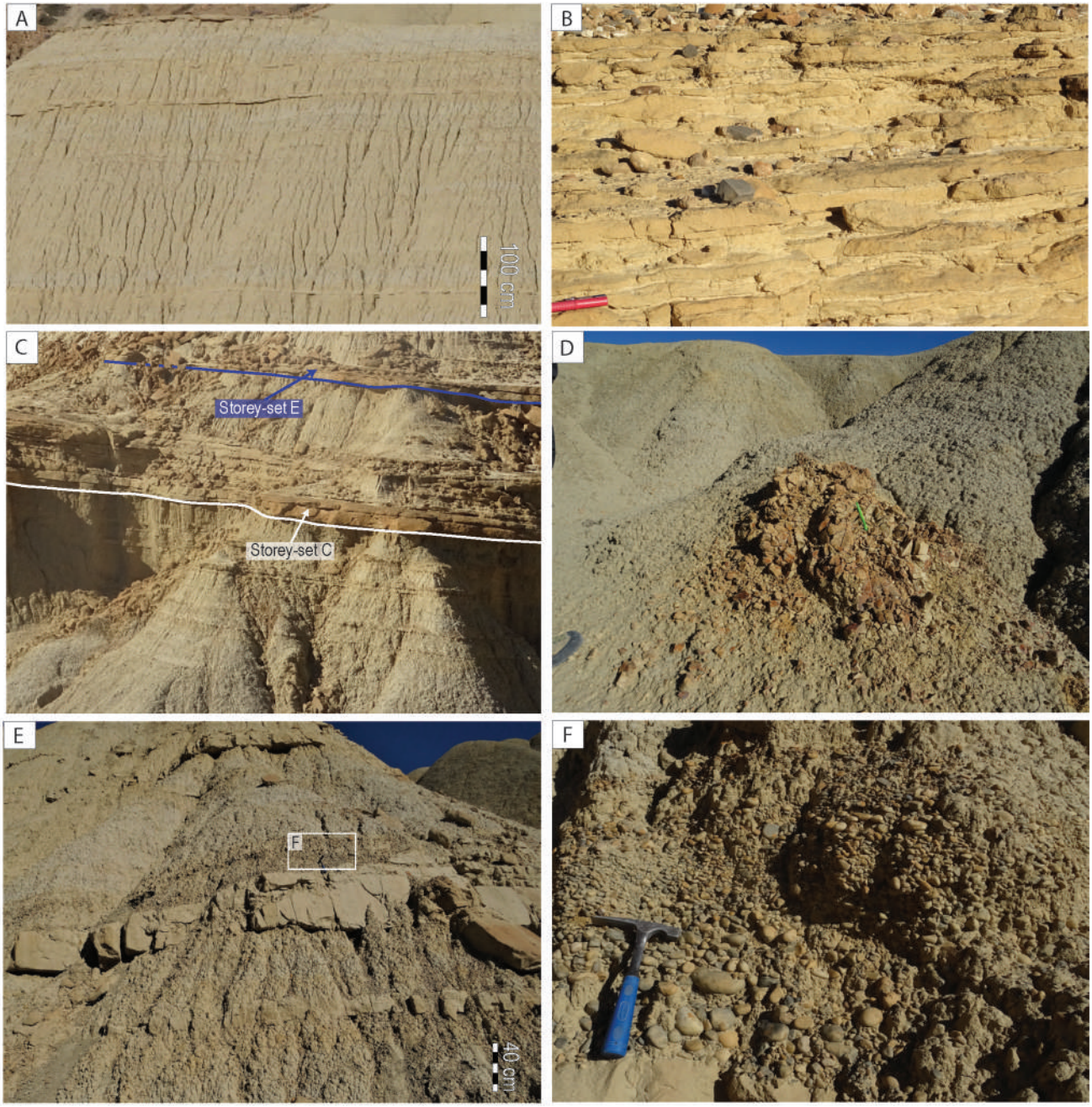

SED_13070_FIG9.tif

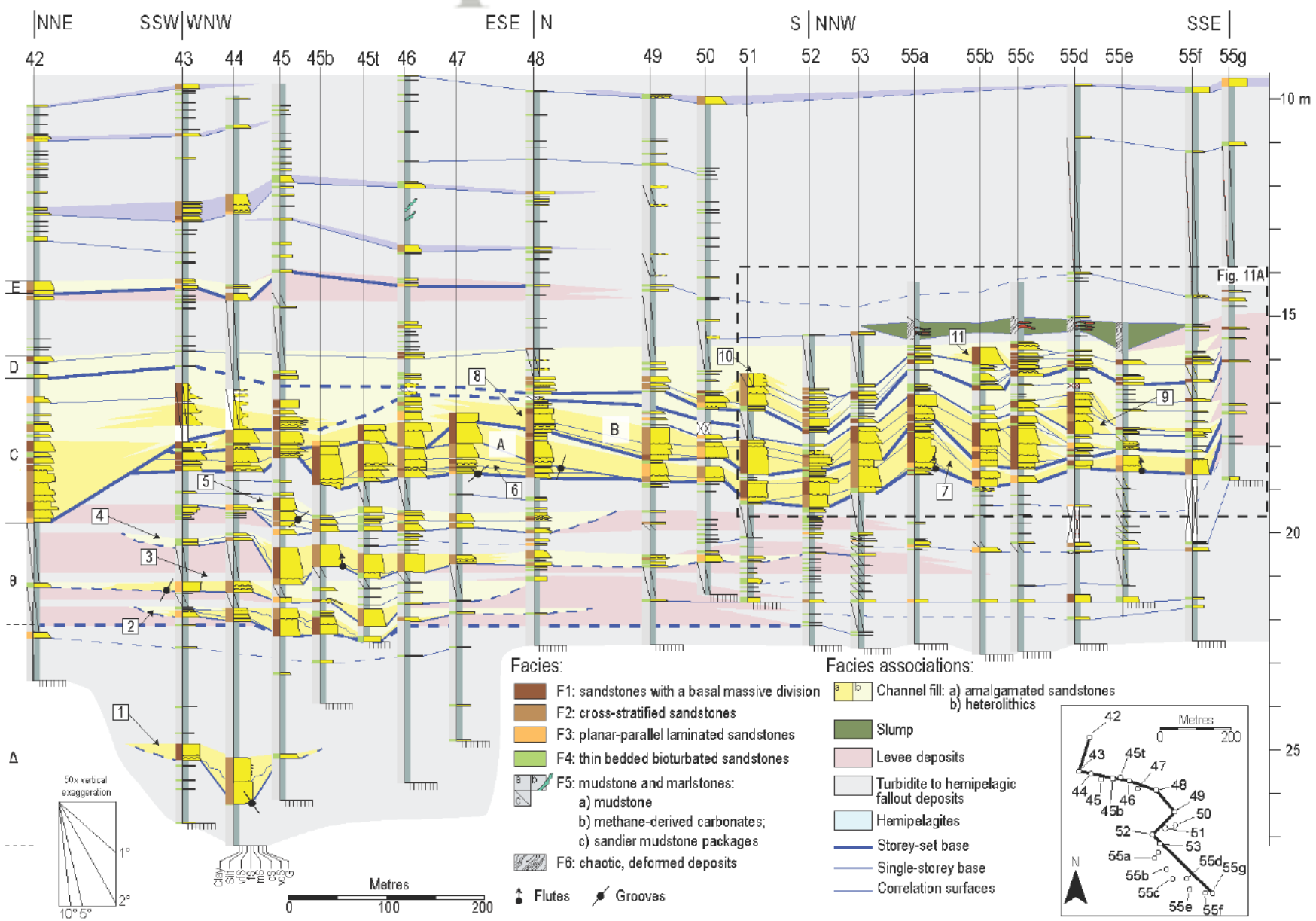

SED_13070_fig10_revSR.tif

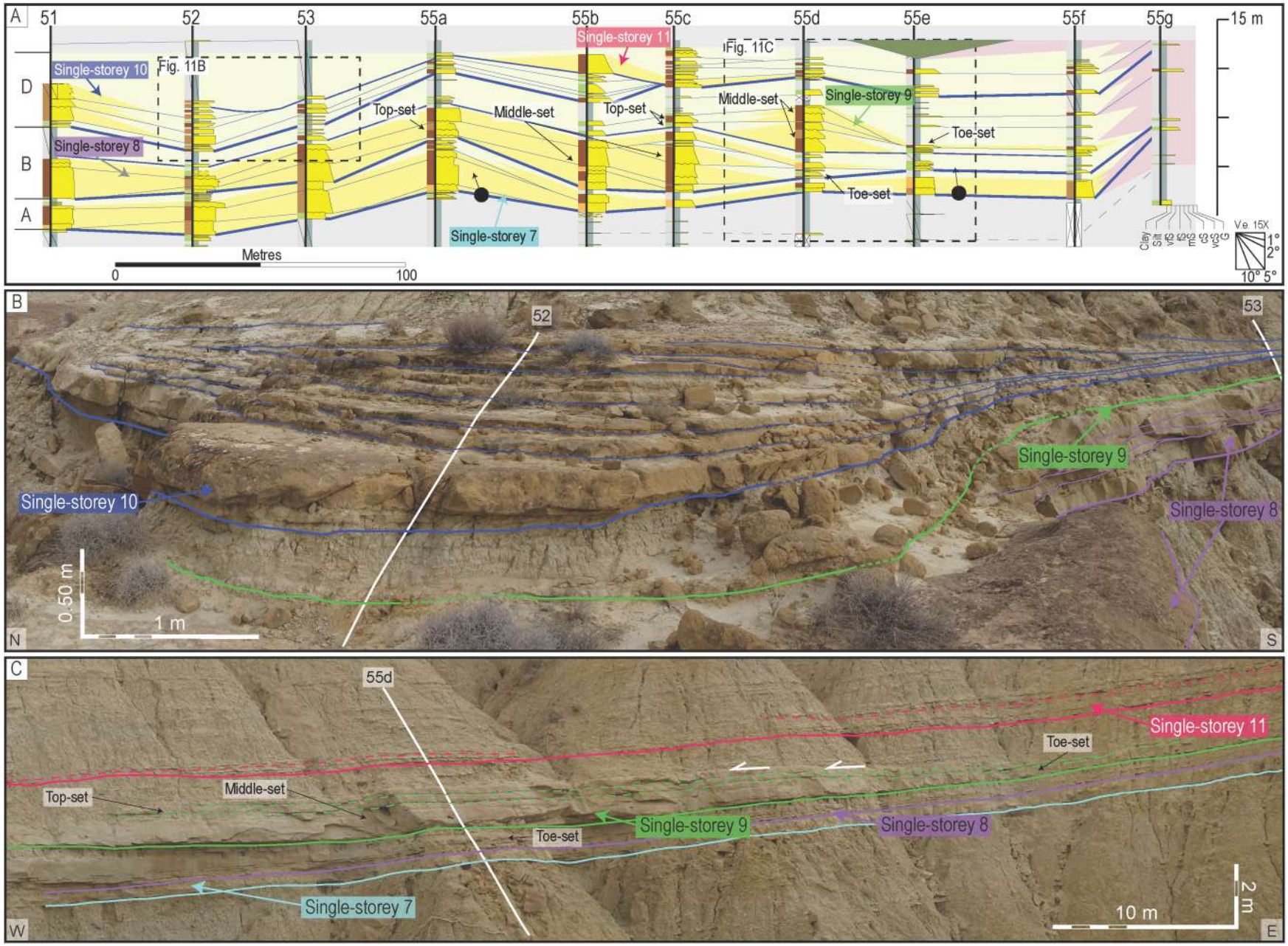

SED_13070_FIG11.tif

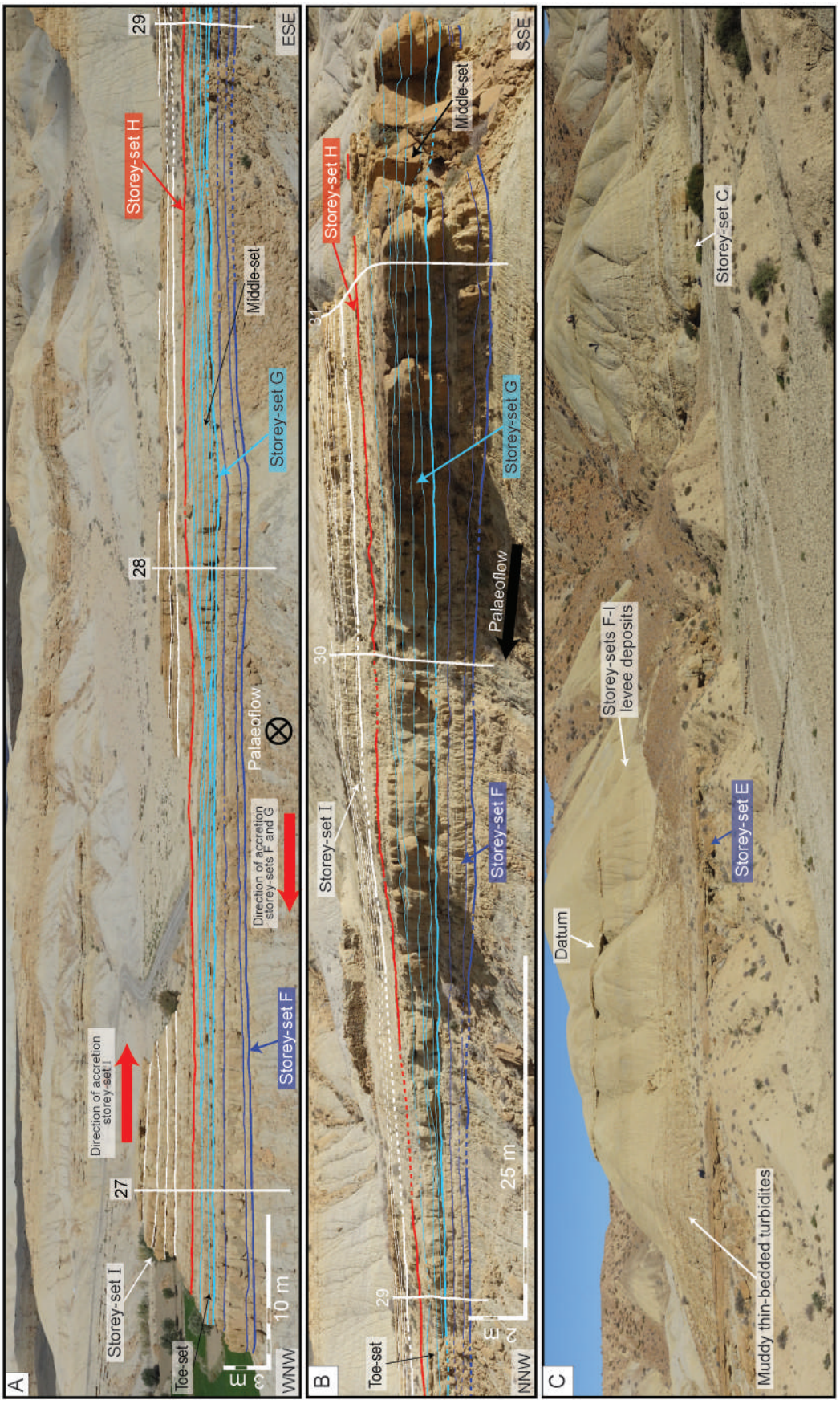

SED_13070_fig12_revSR.tif

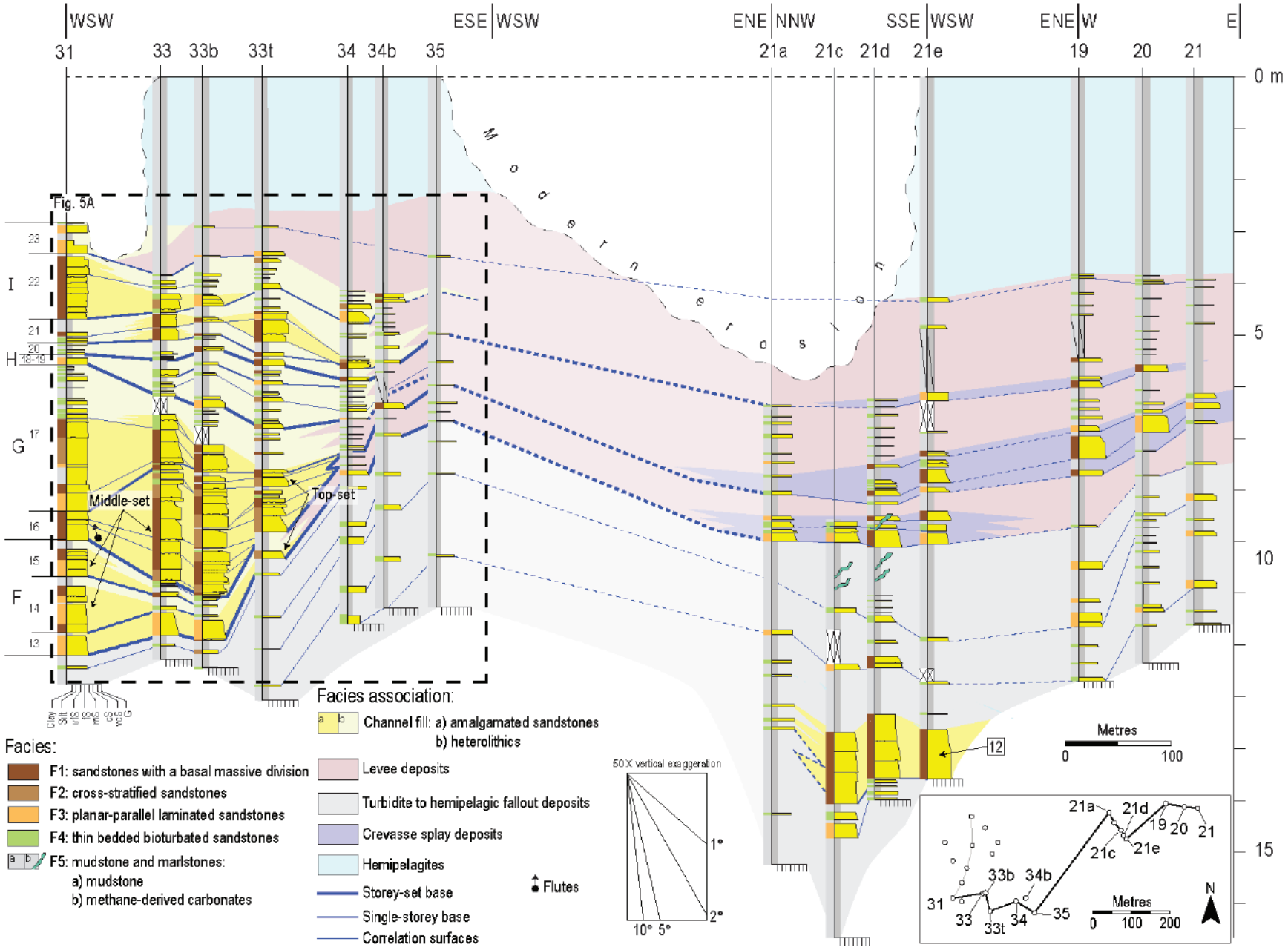

SED_13070_fig13_revSR.tiff

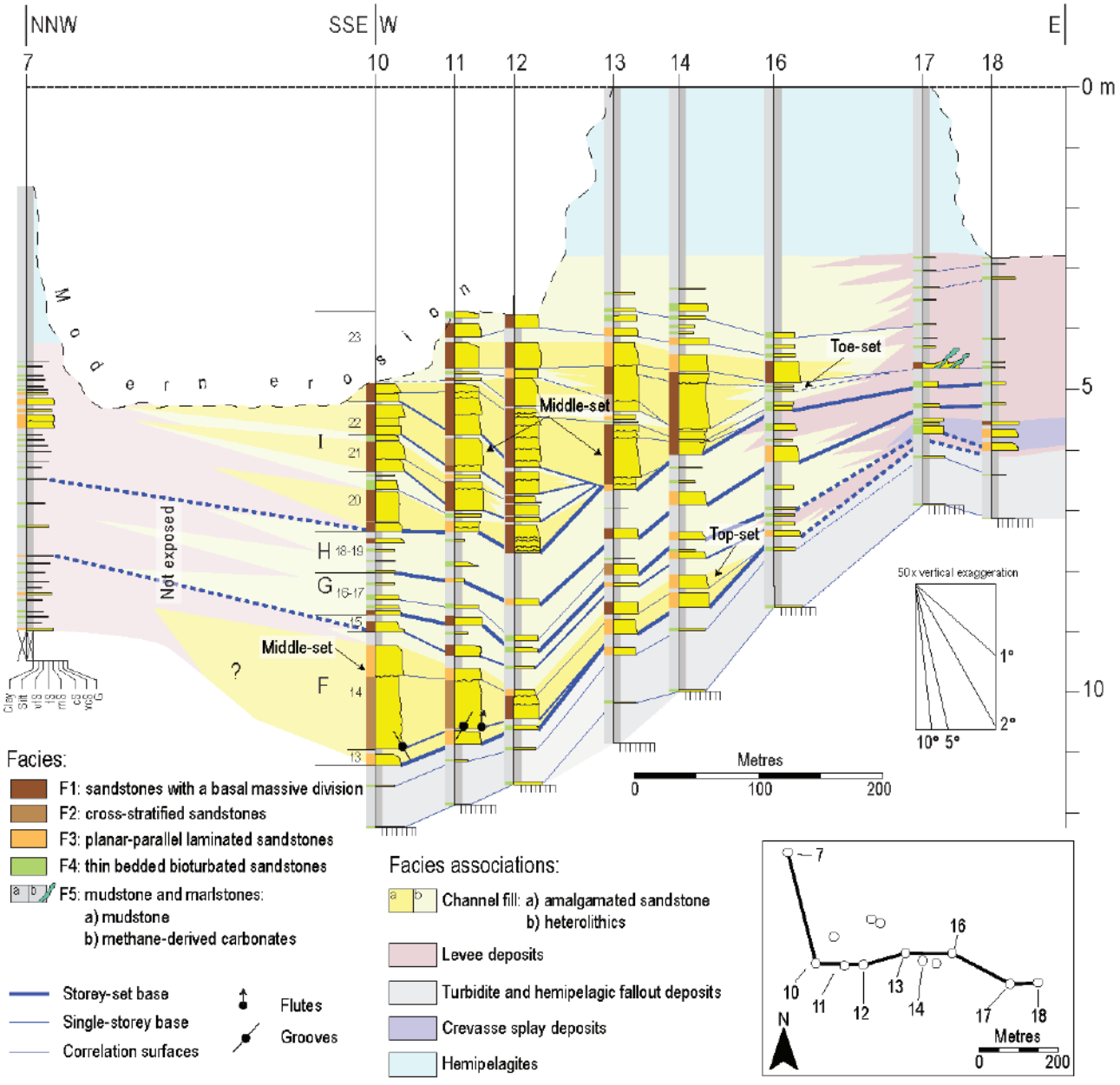

SED_13070_fig14_revSR.tiff

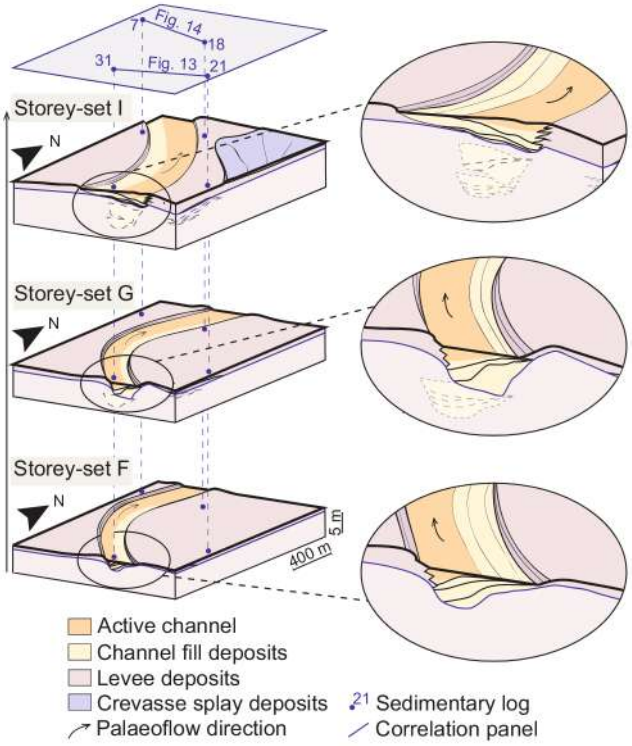

SED_13070_FIG15.tif

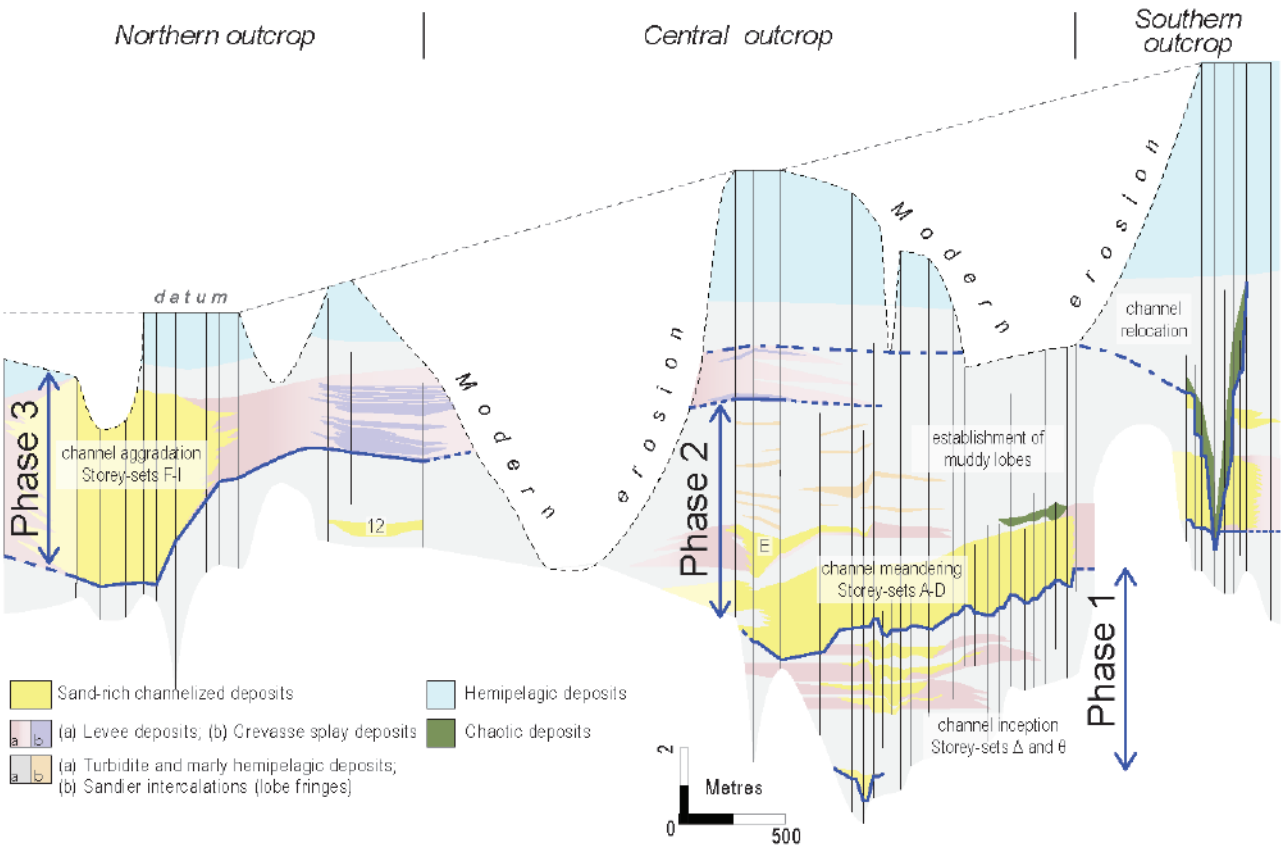

SED_13070_fig16_revSR.tiff

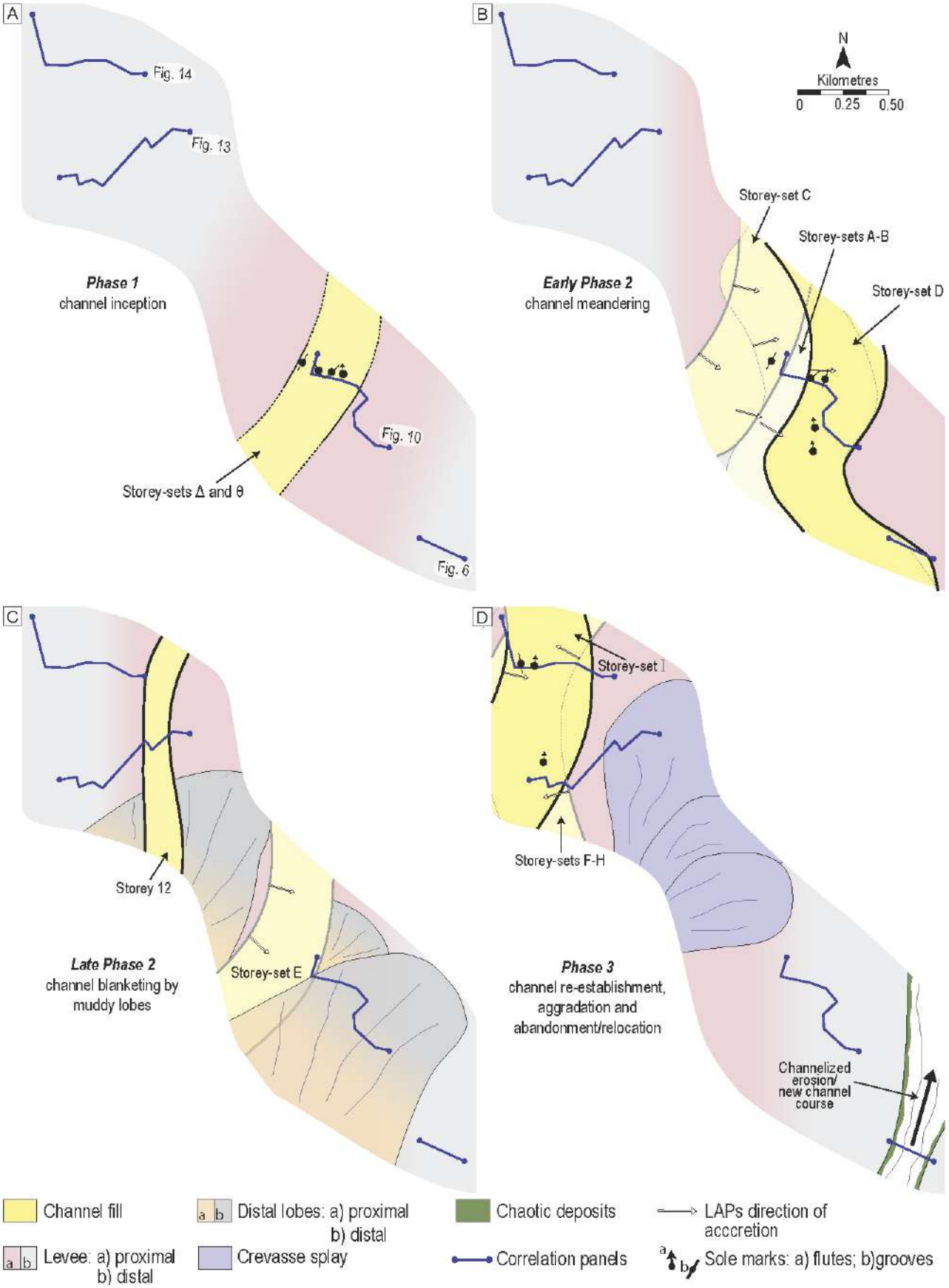

SED_13070_fig17_revSR.tiff